Evaluation study of the Kain-Fritsch convection scheme

Sander Jonkers

De Bilt, 2004

Preface

This thesis rapports on the study I have performed at the KNMI in the period from October 2003 until December 2004. The study and the writing of this thesis in particular embodied the last part of my study 'meteorology and physical oceanography' at the Utrecht University.
I have learned many things during this period. Of course I learned a lot about the topic of this thesis itself and about computer programming; I learned as well what it is about to work on a long project with moments of rapid progress and zero progress.
In retrospect it was a pleasant time at the KNMI. The people I have met at the department of atmospheric research were always willing to help and were the cause of much laughter during numerous coffee breaks, lunches and chats.

I would hereby like to thank everybody who helped me in some way with this project. I want to thank some people in particular as well. First of all, I would like to thank Pier Siebesma for his guidance and very useful comments during the project. Next, Stephan de Roode of the Utrecht University, because of correcting my seminary and giving useful comments, further I would like to thank Sander Tijm for his help with the use of H1D and the comments on the model results, Steve Derbyshire of Met Office, for providing data for the relative humidity sensitivity case and Aarnout van Delden of the Utrecht University for being my second supervisor.

Sander Jonkers,

December, 2004

Summary

Cumulus clouds occur on spatial scales that are too small to be explicitly resolved by state of the art operational weather prediction and climate models. In order to take the effect on the model evolution of these sub-grid convection processes into account a parameterization in the form of a convection scheme is required. A crucial process in a convection scheme is the turbulent exchange of heat, momentum and moisture between clouds and their environment.

A relatively new convection scheme, based on buoyancy sorting, introduced by Kain and Fritsch is used to prescribe this exchange. The main idea of this convection scheme is that at the periphery of the cloud (or updraft) various mixed air parcels are formed that consist of both cloudy and clear air. These mixed parcels can have rather distinct densities. The parcels that are positively buoyant are entrained into the updraft, while the parcels that are negatively buoyant are detrained. The purpose of this study is to evaluate how well the turbulent mixing between clouds and their environment is represented by this buoyancy sorting mechanism. This is done by means of the Simplified Updraft Model, the SUM. This is a single parcel ascent model.
The performance of the SUM is tested by qualitative comparison to Large Eddy Simulation (LES) results. This is done for two distinct cases. The first test is done by means of a typical shallow cumulus case: BOMEX. The aim of this test is to investigate what happens to the updraft profiles if the frequency distribution of the mixed parcels and the amount of the mixed parcels is changed. In the second test case the sensitivity of the Kain-Fritsch scheme to relative humidity is examined. According to Cloud Resolving Model (CRM) - results this sensitivity should be huge, but it is not clearly present in most convection schemes (Derbyshire, 2003).

Contents

1. Introduction

1.1 Convection cells

A primarily vertically organized patch of turbulent air is called a convection cell. Convection cells originate from a forcing. This forcing can be either mechanic or thermal. Thermal forcing is caused by solar radiation that heats up the earth's land surface. As a consequence, the air above the surface is heated as well. The higher the temperature of the air, the lower the air density. Because the surface is heated differentially, some air patches become warmer and hence lighter than their environment, i.e. positively buoyant. Like a hot air balloon this air patch is capable to ascent and to form a convection cell.
Mechanic forcing can e.g. be caused by air convergence. When distinct air flows meet at - for example - the surface the only way is up, to form a convection cell as well.
The maximum depth till which the convection cell can penetrate is determined by several variables, like buoyancy, forced upward momentum and wind shear. Fact is that when a convection cell ascents, the temperature inside the cell decreases with height. So, at a certain height the convection cell can get saturated for moisture and condensation can take place. Due to this condensation, latent heat is released, which causes the temperature inside the cell to increase with height, i.e. the cell is generating buoyancy by itself and can reach a larger depth. These convection cells are known as cumulus (or convective) clouds.
Cumulus clouds can originate from thermal or mechanic forcing, or both. Latent heat release is always involved in the formation of clouds, because clouds consist of condensed water droplets, but it is not a necessity. Latent heat release only enables cumulus clouds to reach deeper.
Cumulus clouds often have a flat base and a top in the shape of a cauliflower, caused by the turbulent motions of the air. There are three sub-categories of cumulus clouds: stratocumulus, shallow cumulus and deep cumulus

Some pictures of these distinct cloud types and their most common region of appearance are shown on the next page.

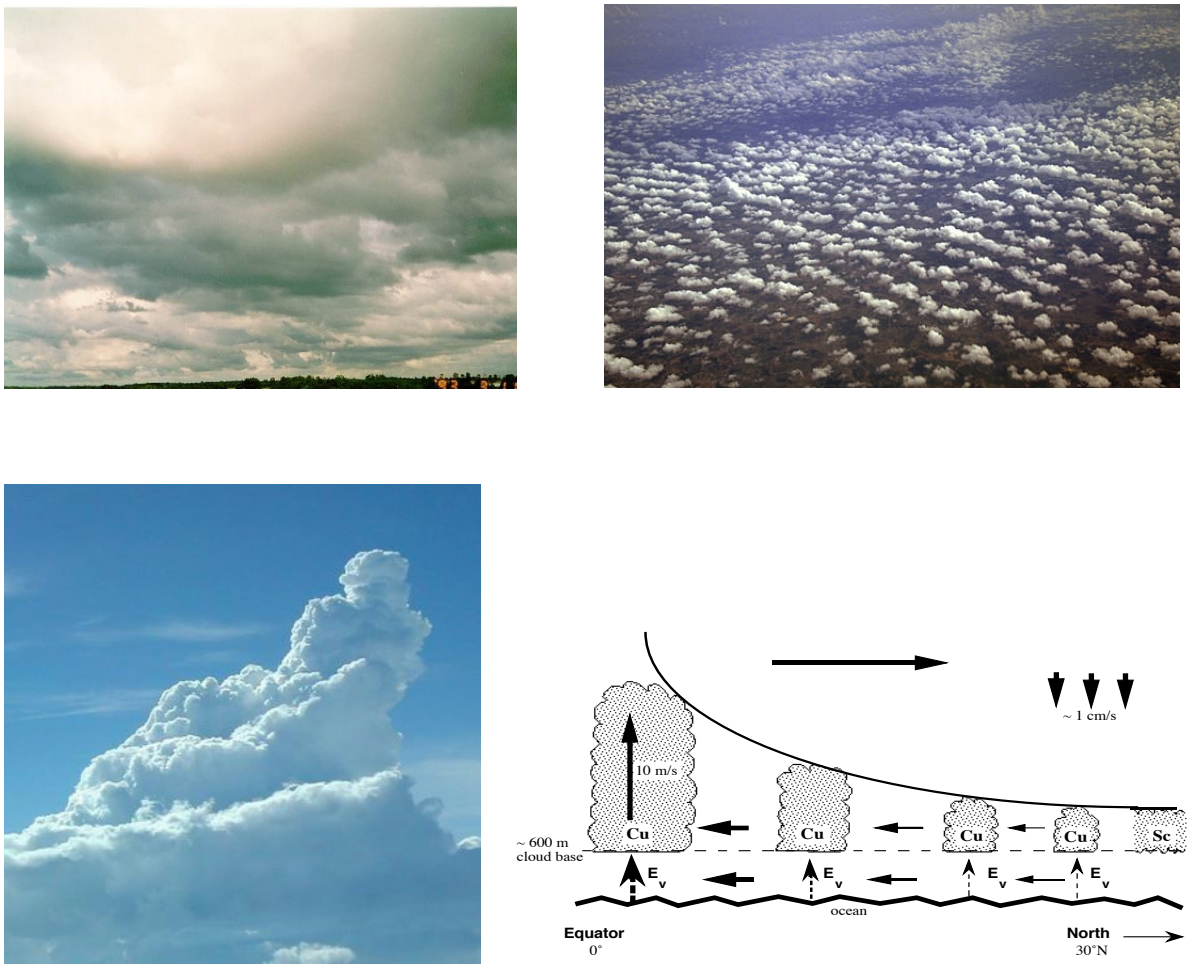

Figure 1. **Upper left:** stratocumulus; **upper right** shallow cumulus; **lower left** deep cumulus with a so-called ice anvil and **lower right:** Cartoon-like cross-section of the Hadley circulation. The thick arrows represent the mass flows, the dotted arrows the evaporation. The cumulus clouds (Cu) increase in height from shallow to deep towards the equator. In the higher latitudes stratocumulus clouds (Sc) are prevailing. For more details on occurrence frequencies, see the ISCCP-archive.

As can be seen in figure 1, cumulus clouds contribute to the Hadley circulation. As is suggested by the cross section, the depth of clouds highly determined by latitude. In reality, the regions of occurrence overlap. Low clouds occur at almost all latitudes except around the equator (ISCCP-archive). Because the characteristics of the distinct cloud types vary considerably, the most important of them are summarized below.

Stratocumulus

These clouds have in general a high cloud cover. They look therefore much wider than thick. Their typical height of occurrence is between 500m and 1 km, but in general this is dependent on the annual and daily cycle. Their occurrence is persistent in the sub-tropics and on the west sides of sub-tropical continents in particular. This is due to relatively cold ocean currents (Neggers, 2002) and large-scale subsidence. Because of their high cloud cover stratocumuli have large impact on the radiation balance. Precipitation can fall out of these clouds, but often in the form of drizzle. Although these clouds look flat and passive, they actually consist of turbulent eddies.

Shallow cumulus

These clouds are also known as fair weather cumuli, because they are non-precipitative and in general have a cloud cover between 20 and 40 %, which is relatively low. In general, the cloud base of these clouds is around 500m and they reach until 2 km height. However, this is as well dependent on latitude and the annual and daily cycle.
In the trade wind areas, these clouds are important for the transport of heat and moisture towards the ITCZ, because they enhance the vertical mixing of warm and moist air. They therefore play a dominant role in the Hadley circulation. Model studies have shown that the presence of shallow cumulus in the trade wind areas seriously enhances the precipitation and variability in the tropics (e.g. Slingo et al, 1994; Gregory, 1997).

Deep cumulus.

The equator-ward flows of the Hadley circulation meet at the ITCZ, where deep cumulus clouds are formed. Although the frequency of occurrence of deep cumuli is the highest in this area around the equator, they can originate at higher latitudes as well.
These clouds can reach heights of more than 10 km, i.e. they can reach until the tropopause. The droplets inside the upper half of these clouds consist for a substantial part of ice particles. The so-called cumulus towers can have a typical anvil-like shape. This is due to the rapid increase in potential temperature around the cloud top at the tropopause. Due to the strong latent heat release, upward velocities in deep cumulus are high and can reach up till 10 m/s. This fast ascent and hence fast cooling of the droplets can cause the forming of hail, thunderstorms and intense precipitation.

1.2 Parameterization

The feature of convection cells and thus of cumulus clouds that should be stressed right now is that they merely occur on relatively small scales, compared to the resolution of a state of the art numerical weather prediction model or climate model. A typical horizontal scale of e.g. a shallow cumulus cloud is on the order of 1 km or less, whereas the highest horizontal model resolution is still around 10 km. Thus, convection cell variables cannot be explicitly resolved as a function of time and space, as is schematically illustrated in figure 2. Therefore, any sub-grid process in a model grid box must be deduced from large-scale, grid box-mean variables that are explicitly resolvable, i.e. sub-grid processes must be parameterized. In the case of shallow cumulus clouds, this means that a whole group of clouds need to be parameterized. These parameterized processes are relatively small in scale, but great in number and hence have a substantial impact on the evolution of the grid box-mean variables.

Because of the awareness of the necessity of sub-grid parameterization and the shortage of observational data, so-called LES (Large Eddy Simulations) are performed to develop and test these parameterizations. These models have a small domain and high resolution. The grid size is much smaller than the characteristic scale of most convection cells. Therefore a LES is capable of explicitly resolving turbulent processes, among which cumulus clouds.

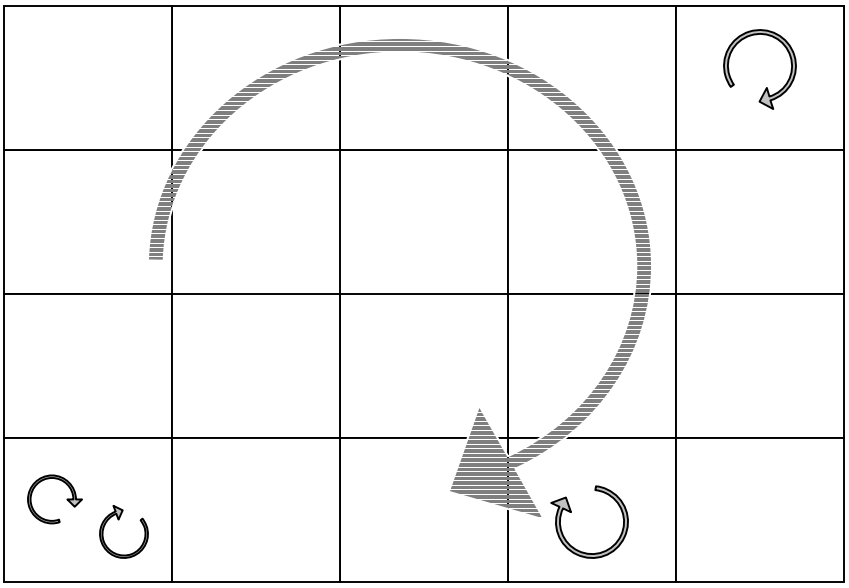

Figure 2. Schematic representation of a sub-grid, unresolved phenomenon (small arrows) and a resolved phenomenon.

1.3 Problem and objectives

In order to parameterize sub-grid convection, a convection scheme is needed.
A convection scheme is a set of relevant physics that can describe the most important properties of convection cells in terms of explicitly resolvable variables.

A common problem of many convection schemes is their insensitivity to the relative humidity of the mean environment of the convection cells. This insensitivity can be illustrated when e.g. the upward transport of cloudy mass: the Updraft Mass Flux (UMF) is considered. In figure 3 the UMF-profiles are plotted when a Cloud Resolving Model (CRM) [1] is used and when convection schemes are used.

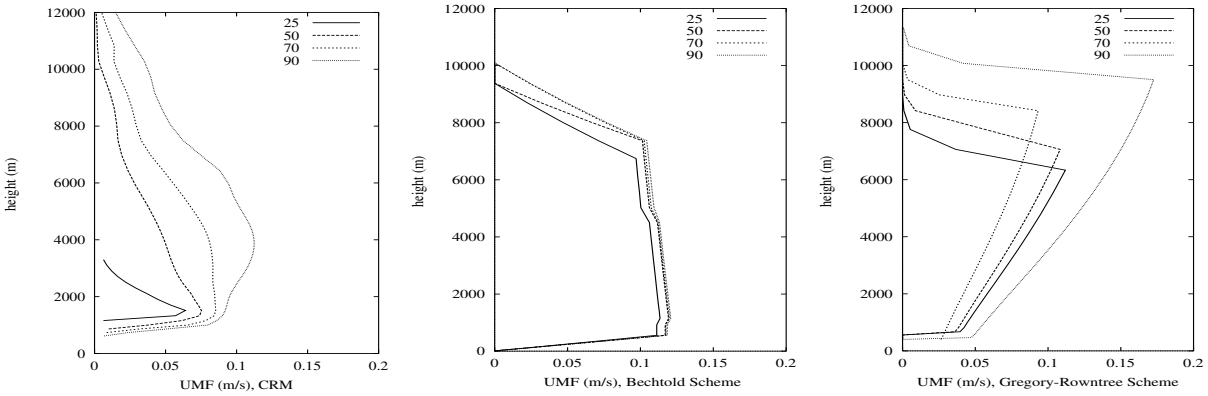

Figure 3. Sensitivity of the mass flux profile when only the relative humidity of the area averaged profile is changed (see keys). The profiles that are obtained by using a CRM, **left** - from MetO - have the status of pseudo observation. The CRM-mass flux profile shows huge sensitivity to relative humidity. The used convection schemes are implemented in Single Column Models (SCM).
Middle: ECMWF-SCM, obtained with the Bechtold convection scheme (Derbyshire, 2003). **Right:** Met Office-SCM, obtained with the Gregory-Rowntree convection scheme (Derbyshire, 2003).
Courtesy: S.Derbyshire and P.Bechtold

A convection scheme that might resemble the CRM-sensitivity to relative humidity is the buoyancy-sorting convection scheme of Kain and Fritsch, 1990. The objective of this study is to perform relative humidity sensitivity tests with the Kain-Fritsch scheme, following Derbyshire, 2003 (chapter 8). In these tests, like in figure 3, the only varied profile is the relative humidity of the mean environment. A sensitivity in particular is the sensitivity of the UMF. This quantity substantially determines - as will be shown later – the impact of clouds on their environment. The sensitivity of the in-cloud values for moisture and heat will be examined as well.

[1] A CRM is more or less the same as a LES, often a CRM has a slightly lower resolution.

Further, more insight needs to be obtained on the role of parameters in the convection scheme itself. These parameters are the maximum amount of air that can mix from the cloud's environment into the cloud itself and the frequency distribution of mixed air parcels at the cloud periphery. For this test a shallow cumulus case dataset is used. Before we proceed with the cloud model and the KF-scheme, first some basic thermodynamics are elucidated.

2. Basic thermodynamic quantities

In this chapter the most important quantities to describe the thermodynamic properties of moist air are mentioned. In principle temperature, pressure and moisture content are the three basic quantities to determine the thermodynamic structure of moist air. Some of these quantities can be modified to make calculations with them more convenient.

2.1 Temperature and moisture

According to the gas law the density of a dry air parcel can be calculated when its temperature and pressure are known. When the air contains moisture, matters become more complicated, because water vapour has a different (lower) density than dry air.
In order to determine the density of moist air from the dry air gas law, the so-called virtual temperature is defined. This is the temperature dry air must have in order to have the same density as moist air, with given moisture content. It is written as

$$T_v = T\left[1 + 0.61 q_v - q_l\right]. \tag{1}$$

In the derivation of T_v, given in appendix A.1 it is clear that for this temperature the dry air gas law applies. Further, it is clear that T_v increases when the water vapour mixing ratio q_v increases and decreases when the liquid water-mixing ratio q_l increases.
In appendix A.2 the derivation of the saturation-mixing ratio q_s with respect to water or ice is given. Water vapour condensates, to form liquid water or ice, when its specific humidity (A.2) exceeds this saturation ratio, which is given by

$$q_s = \varepsilon \frac{e_s}{p + e_s(\varepsilon - 1)}, \tag{2}$$

where e_s is the saturation vapour pressure (A.2), p is the pressure and ε equals 0.62. The saturation vapour pressure is a strong function of temperature, so in a convective process face change can occur. The specific mixing ratios q_v and q_l are dependent on phase changes. The sum of both the mixing ratios q_t is not. It is conserved under adiabatic processes.

The other mayor advantage of the use of q_t is that this quantity can be linearly mixed (A.3). Because of phase change and the inherent latent heat exchange, temperature cannot be linearly mixed. To make linear mixing of temperature under constant pressure possible, the liquid water temperature T_l is defined. This quantity (A.3) is conserved under adiabatic phase change as well and is given by

$$T_l = T - \frac{L_0}{c_{pd}} q_l . \tag{3}$$

As already mentioned, vertical motion occurs during convection, and thus the ambient pressure in an air parcel changes during convection. When the parcel is - e.g. - ascended vertically the pressure inside the parcel drops. When the ascent is assumed to be adiabatic, the temperature inside the parcel drops as well, due to expansion. A quantity that is conserved under adiabatic pressure change / vertical displacement is the potential temperature θ (A.3) defined as

$$\theta = T(\frac{p_0}{p})^{\kappa} = T\pi^{-1}. \tag{4}$$

In which p_0 is a reference pressure, κ equals 0.29 and π is the so-called Exner function. This quantity is not conserved when phase changes are included. The quantity that is conserved for adiabatic pressure change *and* phase change is the liquid water potential temperature θ_l (A.3), approximated by

$$\theta_l \approx \theta - \frac{L_0}{c_{pd}\pi} q_l . \tag{5}$$

Analogous to the total water content q_t, this quantity can be linearly mixed.

The virtual potential temperature θ_v can be derived analogous to (4) and (1). We find

$$\theta_v = \theta[1 + 0.61 q_v - q_l] \tag{6}$$

The difference in the virtual (potential) temperature of a parcel, and that of its environment determines the buoyancy of a parcel.

The difference in vertical gradients of the potential temperature of a parcel, and that of its average environment determines the stability of the atmosphere. When, for example, a saturated parcel has a stronger increase of temperature with height than its environment, but a weaker or no increase (compared to its environment) when it is unsaturated, the atmosphere is called conditionally unstable (Siebesma, 1997).

3. A cloud model

In this chapter the typical vertical structure of an atmosphere in which cumulus convection occurs will be examined. This will be done by means of a relatively simple cloud model.

3.1 The single parcel method

Many in-cloud fields and other cloud properties are determined by the properties of the atmosphere outside the cloud. This is shown in figure 4. It shows an idealized vertical virtual potential temperature profile of a typical convective atmospheric layer and that of an ascending parcel that represents a convection cell.

The parcel ascends from the surface. Just above the surface, the environmental profile of θ_v is decreasing with height, because the air is heated by radiation from the surface. Above this thin layer there is a well-mixed boundary layer in which θ_v of the environment is constant with height. When we assume the parcel to be adiabatic it experiences positive buoyancy in this layer. During the ascent, the parcel cools down due to adiabatic expansion. When it becomes saturated, it has reached its Lifting Condensation Level (LCL). In general, the parcel is negatively buoyant at this altitude, but it can ascent in this layer at the cost of its vertical velocity. Because of the release of latent heat, the virtual potential temperature of the parcel is increasing with height from the LCL. If the environment is conditionally unstable, the parcel can reach a level at which it becomes again positively buoyant: the Level of Free Convection (LFC). Above this level the parcel is, due to its onboard heat generator capable to reach the Level of Zero Buoyancy (LZB).
At this level the parcel becomes negatively buoyant once more. This is usually caused by an increase of the vertical gradient of environmental virtual potential temperature. The parcel can penetrate above this level, again at the cost of vertical velocity, which is called overshooting. The cloud top is usually defined as the height at which the vertical velocity becomes zero. The LCL is a rather good estimate for the cloud base.

The layer between the LCL and LFC in which the parcel is negatively buoyant prevents parcels with lower kinetic energies or vertical velocities to penetrate through the LFC. This potential barrier is the cause for the formation of separate clouds. When there is no such barrier at all, clouds can form a homogeneous blanket.

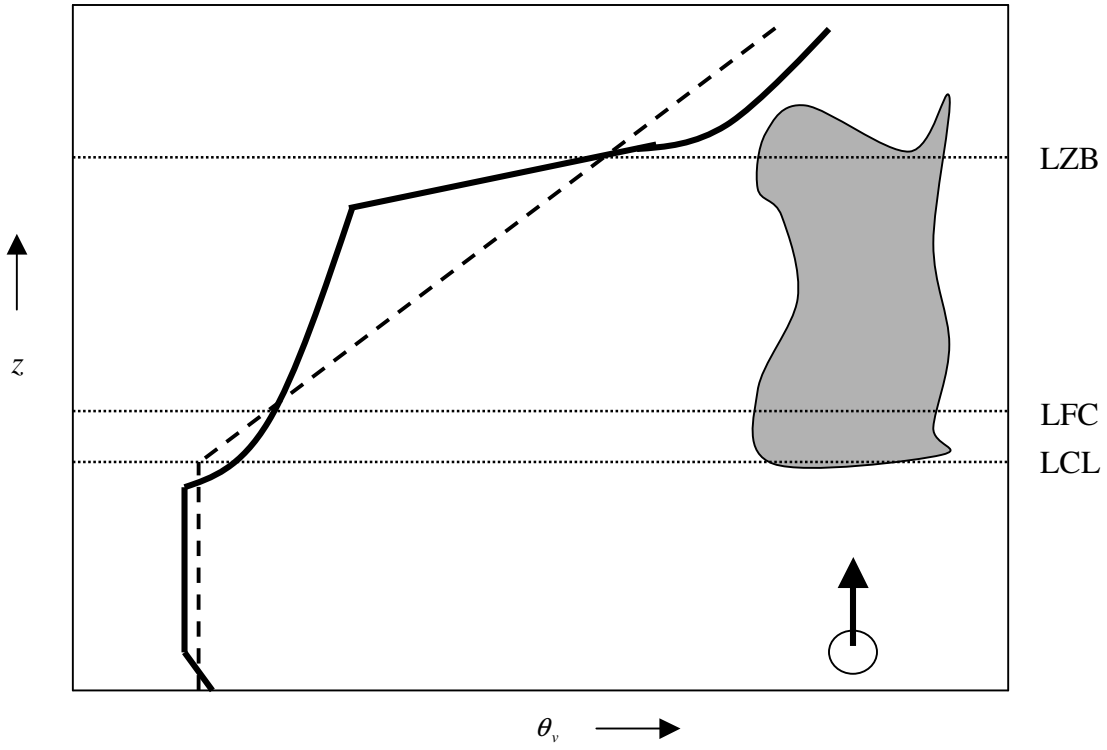

Figure 4. Schematic virtual potential temperature vertical profiles of the ascending parcel (dashed) and of its environment (solid). Note the overshooting above the LZB.

4. Cloud mixing

The behavior of clouds could be described rather well by the before mentioned adiabatic single parcel method if they were behaving adiabatic as well. This is obviously not the case in reality. It was shown (Stommel, 1947) that clouds continuously mix air with their environment. It was shown by Warner, 1955 that the liquid water content in clouds is substantially lower than the adiabatic parcel method prescribes. This is a strong indication for the mixing of cloudy air with air from the unsaturated environment. Because the difference in liquid water mixing ratio between that of clouds and that of the adiabatic parcel method increases with height (e.g. Jonas, 1990), it can be concluded - when there is no precipitation - that clouds are diluted continuously with environmental air. This dilution is caused by entrainment. It has substantial impact on most of the in-cloud fields and the maximum depth a cloud can reach. The transport in opposite direction: of cloudy air into the environment is named detrainment. The KF-convection scheme offers a method to prescribe the mass exchange between clouds and their environment. This mass exchange transports moisture and temperature as well. Before the KF-scheme can be implemented in the cloud model, equations that describe the

vertical in-cloud profiles as a function of entrainment, detrainment and the environment are derived from the large-scale continuity equations for θ_l and q_t.

4.1 The approximated vertical profile equations

In appendix A.4 the updraft mass flux M is defined as $\rho \cdot a \cdot w$, in which ρ is the density of the cloudy air, a the fractional cloud cover and w the in-cloud vertical velocity. The vertical profile of M can be derived in terms of the entrainment E and detrainment D. In the end, we can write

$$\frac{\partial M}{\partial z} = E - D. \tag{7}$$

And when we write ϕ for both θ_l and q_t, we can write the upward flux of ϕ in terms of M, E and D as

$$\frac{\partial M\phi_c}{\partial z} = E\bar{\phi} - D\phi_c. \tag{8}$$

Where the overbar denotes a spatial average and the subscript c the in-cloud value.

The entrainment and detrainment can be parameterized as a fraction of the local mass flux or as a fraction of the mass flux at the cloud base. The common choice is the local mass flux, whereas in KF a fraction of the mass flux at the cloud base is used. So, we obtain the following equations

$$\begin{aligned} E &= \varepsilon M, \\ D &= \delta M, \end{aligned} \tag{9}$$

or

$$\begin{aligned} E_{KF} &= \varepsilon M_b, \\ D_{KF} &= \delta M_b. \end{aligned} \tag{10}$$

In which ε and δ denote the fractional entrainment and detrainment, respectively. The subscript *b* denotes the cloud base. When we apply (9), we find for the vertical mass flux profile

$$\frac{\partial M}{\partial z} = M(\varepsilon - \delta). \tag{11}$$

The vertical dilution equation for ϕ_c can be written as

$$\frac{\partial \phi_c}{\partial z} = \varepsilon(\bar{\phi} - \phi_c). \tag{12}$$

When we apply (10), we find, after substitution

$$\frac{\partial M_{KF}}{\partial z} = M_{KF}(\varepsilon_{KF} - \delta_{KF}). \tag{13}$$

And for the dilution equation for $\phi_{c,KF}$

$$\frac{\partial \phi_{c,KF}}{\partial z} = \varepsilon_{KF}(\bar{\phi} - \phi_{c,KF}). \tag{14}$$

with the so-called KF fractional entrainment and detrainment ε_{KF} and δ_{KF} given by

$$\begin{aligned} \varepsilon_{KF} &= \varepsilon \frac{M_b}{M_{KF}}, \\ \delta_{KF} &= \delta \frac{M_b}{M_{KF}}. \end{aligned} \tag{15}$$

Note that according to (12) the updraft properties ϕ_c are independent of the detrainment, which is intuitively plausible. When we have the boundary conditions of ϕ_c and M, we also have their profiles, given values of ε and δ. According to (14), updraft properties $\phi_{c,KF}$ are dependent on both entrainment and detrainment. As will be discussed later, this choice of parameterization (10) has significant impact on the updraft profiles.

5. The Kain-Fritsch scheme

Now that that the vertical profile equations that can parameterize the updraft properties are obtained, we may start wondering what values to choose for ε and δ. In most parameterizations ε and δ are chosen to be constant with height. When we consider (12) it is clear that ε^{-1} has unit *m* and can be interpreted as a typical vertical relaxation height scale of the cloud properties ϕ_c. So, when we take 1-10 km as a typical cumulus cloud depth, a first guess for the value of ε is between 10^{-3} and 10^{-4} m^{-1}.

The fractional detrainment δ is often chosen to be a constant fraction of ε (i.e. Johnson 1977; Lord 1982; Frank and Cohen 1985). When ε and δ are preset, then - according to (11) - the vertical gradient of the mass flux is preset as well. This will yield to less sensitivity of the magnitude of the mass flux to changes in temperature and moisture in the environment. This is not realistic as can be seen in figure 3. The convection scheme of Kain and Fritsch, from now on KF, might solve this sensitivity problem.

The KF-scheme is based on the past observation (e.g. Rogers et al. 1985; Paluch and Baumgardner 1989) that suggest that turbulent eddies at the edge of the cloud continuously create mixtures that consist of various fractions of clear and cloudy air. The buoyancy of the mixed air can be quite different than the mean buoyancy of the cloud air itself. Figure 5 shows the difference in virtual temperature of a mixed parcel and the environment of the cloud as a function of the fraction of environmental air mass χ. Note that χ ranges from 0 to 1 and that a parcel with χ equal to 1 consists of environmental air only. For the ambient conditions, all mixtures that contain more than 45% of environmental air are negatively buoyant and mixed parcels that contain less than 45 % environmental air remain positively buoyant, with respect to the environment.

There are several remarks that can be made on this picture. First it should be stressed that the virtual temperature of the mixed parcel for values of χ greater than χ_c becomes less than the virtual temperature of both the clear air parcel and the cloudy air parcel. This is caused by the mixing of the oversaturated cloudy air with unsaturated air from the environment. The evaporation of the condensed water and the concomitant latent heat exchange makes the temperature of the mixture to fall more rapidly as a function of χ than when only unsaturated air is involved. When all the liquid water is evaporated, the virtual temperature difference makes a kink and becomes equal to zero when χ equals 1, as it should be by definition. This kink is the consequence of the fact that the mixed parcel is either saturated or unsaturated. However, the exact shape of the curve given in this picture is just the result of the specific conditions given.
In the KF-scheme it is assumed that all negative buoyant mixtures are detrained and all positive buoyant mixtures are entrained. The fraction of the mixed parcel that entrains detrains is therefore mainly determined by χ_c.

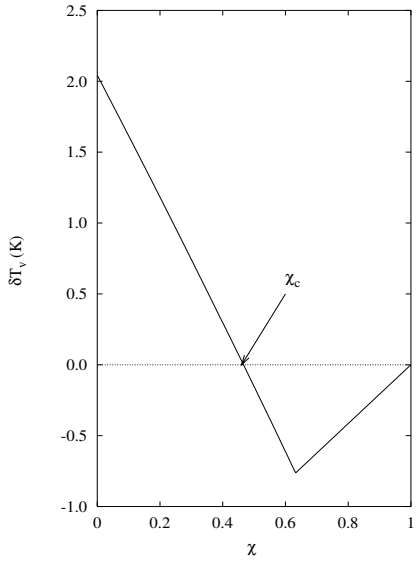

Figure 5. Difference between the mixed parcel virtual temperature and environmental virtual temperature. The ambient conditions are: pressure 600mb, environmental temperature 273 K, relative humidity 70 %, updraft temperature 275 K and an updraft liquid water content of 2 g kg^{-1}.

The exact relation between χ_c and both the entrainment and detrainment will be given later, but a larger χ_c yields obviously a larger entrainment and a smaller detrainment. The methods that can be used to determine χ_c are discussed in A.6.

5.1 Entrainment and detrainment prescription

The single parcel ascent model, with the KF-scheme implemented in it is from now on called the Simplified Updraft Model (SUM).The KF-scheme assumes that all negative buoyant mixtures detrain and all positive buoyant mixtures entrain. In order to implement the relation between χ_c and the entrainment and detrainment in the SUM, first a magnitude of the parcels that are involved in the mixing has to be set.

This mixed parcel consists of a fraction environmental and a fraction cloudy air.
The fraction environmental air is called the Rate of Environmental Inflow or REI and is equal to the upper bound of the entrainment. This rate is often chosen to be constant with height, scaled with the radius R (e.g. Simpson, 1983) or depth H (e.g. Bretherton and McCaa, 2003) of the cloud. When the REI is written as dM_e we can write

$$dM_e = M_{uo}\frac{0.2}{R}dz = M_{uo}\cdot\varepsilon_0\cdot dz \tag{16}$$

where M_{uo} is the radius and mass flux of the cloud at the cloud base and dz is a unit height interval. This is the default inflow rate in the KF-scheme.
The scaling of Bretherton and McCaa is given by

$$dM_e = M_u\frac{15}{H}dz = M_u\cdot\varepsilon_0\cdot dz \tag{17}$$

in which M_u equals $M(z)$. The important difference between (16) and (17) is that in (16) the inflow rate is a constant fraction of mass flux at the cloud base, whereas in (17) it is a fraction of the local mass flux. Because (17) is intuitively more plausible than (16), we take (17) to specify the inflow rate. The parameter that is yet to be chosen is the fractional inflow rate ε_0.

As can be intuitively understood, the ensemble cloud cover in a cumulus cloud dominated layer in general decreases with height. This is schematically shown in figure 6. It is clear from LES-results that this decrease with height contributes to a fractional entrainment that is inversely proportional with height (Siebesma, 2002). This result is motivating to choose ε_0 proportional to the inverse of the height as well. Hence, we write

$$\varepsilon_0 = \frac{c}{z} \tag{18}$$

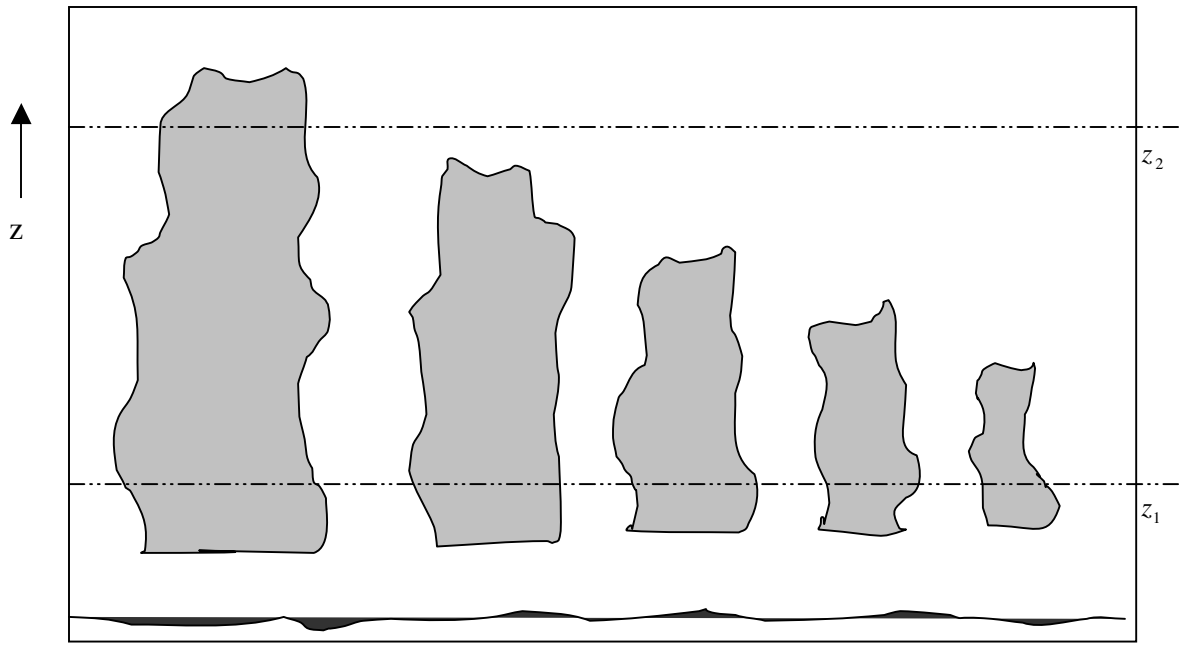

Figure 6. Schematic vertical section of a cumulus cloud layer. Some clouds reach deeper than others, this means that the averaged cloud cover at a horizontal area at height z_1 is greater than that at height z_2; *i.e.* the ensemble cloud cover decreases with height.

The amount of environmental air that is available for mixing is set when the REI is set. For the moment we assume that the amount of cloudy air dM_u that is envolved in the mixing is equal to the amount of environmental air. This yields a total mass of mixed air dM_t of $2\varepsilon_0 M_u$, consisting of several distinct parcels. The amount of parcels that is entrained is the amount with a mixing fraction χ smaller than χ_c. In general, some mixed parcels occur more often than others. Because of this, each mixed parcel has a distinct contribution to the amount of air that is entrained / detrained. In order to implement the frequency of occurrence, a probability density function $p(\chi)$ is attributed to the mixtures. There is no empirical evidence to favor one PDF or the other, so the best choice is the simplest one, or the one that makes intuitively sense. In the standard KF formulation a Gaussian PDF is chosen. This makes intuitively sense, because - in reality - there are obviously many distinct influences on the mixed parcels. This makes the assumption that they are Gaussian distributed plausible.

The simplest choice is a uniform PDF (Bretherton and McCaa 2003). This states that all the mixtures are equally likely to be found. In Appendix 7 it is shown how ε and δ can be derived in terms of ε_0 and χ_c. In general for any PDF $p(\chi)$ we find.

$$\varepsilon = \varepsilon_0 \frac{dM_t}{dM_u} \int_0^{\chi_c} \chi p(\chi) d\chi$$
$$\delta = \varepsilon_0 \frac{dM_t}{dM_u} \int_{\chi_c}^{1} (1-\chi) p(\chi) d\chi \tag{19}$$

When the uniform PDF (A.7) is applied, we find

$$\varepsilon = \varepsilon_0 \chi_c^2,$$
$$\delta = \varepsilon_0 (1-\chi_c)^2. \tag{20}$$

The Gaussian PDF (A.7) is given by

$$p(\chi) = \frac{6}{0.97\sqrt{2\pi}} \cdot (e^{-\frac{(\chi-m)^2}{(\sqrt{2}/6)^2}} - e^{-4.5}) \tag{21}$$

The concerning expressions for ε and δ are not easy to derive. The resulting mapping of ε and δ is given in figure 7.

When it is assumed that parcels that consist mainly out of cloudy air are more likely to be found, The PDF for the mixed parcels is asymmetric. For the PDF given in (A.7) this yields

$$\varepsilon = \varepsilon_0 (\chi_c^4 - 2\tfrac{2}{3}\chi_c^3 + 2\chi_c^2)$$
$$\delta = \varepsilon_0 (1-\chi_c)^4. \tag{22}$$

With expression (20), the mass flux equation becomes

$$\frac{\partial M}{\partial z} = \varepsilon_0 M (2\chi_c - 1). \tag{23}$$

So, the mass flux will increase (decrease) with height when χ_c is greater (smaller) than 0.5. This is the case for all PDFs that have an expectation value of 0.5. When the asymmetric PDF is concerned the mass flux will increase (decrease) with height when χ_c is greater (smaller) than 0.37.

In figure 7, the normalized fractional entrainment and detrainment for distinct PDFs are illustrated.

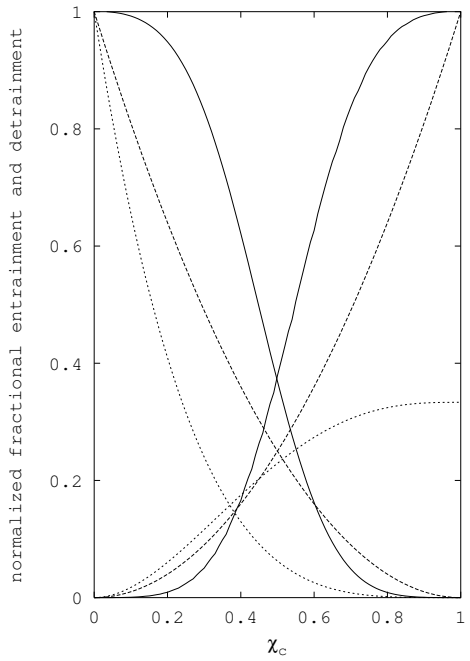

Figure 7. Fractional entrainment (increasing with increasing χ_c) and detrainment divided by ε_0 i.e. $\varepsilon/\varepsilon_0$ and δ/ε_0, for a Gaussian (solid lines), straight (dashed lines) and asymmetric (dotted lines) PDF for the mixed parcels. When χ_c equals 0.5 the fractional entrainment and detrainment are both 37 % of the inflow rate for a Gaussian distribution and 25% in case of a straight distribution. In case of the asymmetric PDF the entrainment exceeds the detrainment at $\chi_c \approx 0.37$.

It is clear from figure 7 that the PDF substantially influences ε and δ. Typical values of χ_c are between 0.4 and 0.6. As can be seen, ε resulting from the asymmetric PDF starts diverting from the values for ε resulting from the symmetric PDF's when χ_c becomes greater then 0.45. This is because the frequency of occurrence for mixed parcels with greater values for χ becomes much lower when the asymmetric PDF is concerned and because parcels with low values for χ hardly contribute to ε. Further, when the asymmetric PDF is concerned, the maximum amount of air that is entrained is $0.33\delta M_u$; see (22). When the symmetric PDF's are concerned the maximum amount is δM_u. This is because the total amount of environmental air in the mixtures equals the total amount of updraft air - in the mixtures - when the PDF is symmetric. When the asymmetric PDF is concerned, the amount of environmental air equals $0.33\delta M_u$.

The maximum amount of air that can be detrained is always δM_u. This can be seen in figure 7. Whatever PDF is chosen, when χ_c equals zero, all updraft air is detrained. This means that δ equals ε_0 when χ_c equals 0 for any PDF.

Another remark is that ε and δ for do not add up to ε_0, except when χ_c equals zero or one. This feature of the mixing scheme has no further consequences, but some explanation on it is given in (A.7).

6. Experiment set up

The performance of the SUM is tested in a typical shallow convection case and in a relative humidity sensitivity test case. The aim of the first test is to obtain insight in the consequences for the in-cloud profiles when the PDF for the mixed parcels and the inflow rate are changed. The SUM in-cloud profiles are compared to in-cloud profiles resulting from LES.
In the relative humidity case the sensitivity of the SUM in-cloud profiles to the relative humidity of the environment is tested. The in-cloud profiles of the SUM are again compared to the in-cloud profiles resulting from CRM, but now in a more qualitative way.
In both the test cases the environmental profiles are in steady state. This means - according to (a.33) - that

$$\frac{\partial \overline{\phi}}{\partial t} = -\frac{\partial M(\phi_c - \overline{\phi})}{\partial z} + \overline{S} \approx 0.$$

This means that the impact of clouds on $\overline{\phi}$ and the large scale forcing $\overline{S}$ on $\overline{\phi}$ balance each other. Because of this, it is reasonably to assume that an instantaneous in-cloud profile, calculated by the SUM, is representative for a time-averaged LES profile. Next, in figure 8, the model set up is summarized.

	ϕ_c	M	ε, δ	w	precipitation	freezing
Above the LZB	(12)	(13)	(a.55)	(a.54)	(a.53)	(a.9)
In the Cloud	(12)	(13)	(19)	(a.54)	(a.53)	(a.9)
At the LCL	C_{st}	CRM/LES -value	(19)	1. m/s	None	None
Under the cloud	C_{st}	0.	0.	0.	None	None
Surface	ϕ_e	0.	0.	0.	None	None

Figure 8. In the SUM, equations (11) and (12) are integrated upward. At each layer, starting just above the LCL, ε and δ are calculated according to (18). The fractional detrainment above the LZB is calculated according to (a.55)

As is suggested by figure 8, sub-cloud ascent is undiluted (or adiabatic). In the next chapter it will be discussed why this assumption has no substantial consequences. As already shown, the parameter that is yet to be set is the fractional inflow rate ε_0.
We are especially interested in the performance of the SUM when ε_0 is chosen to be proportional to the reciprocal height. According to (16) and (17), ε_0 scales with the inverse of the radius or depth of the cloud. Hence, when ε_0 is set this way, shallow and deep cumuli need different values for ε_0 to be well parameterized. When ε_0 is chosen according to (18), an expression for ε_0 might be found that applies well for both shallow and deep convection.

When deep convection is considered, some physical processes that are of less importance in the shallow convection case have to be included in the SUM. These processes are freezing and precipitation. Freezing causes the release of latent heat and precipitation forms a sink of condensed water. Both these processes have no important role in shallow cumulus, because these clouds are not deep enough to form precipitation and cannot - for the case that is considered in this test - reach altitudes were the temperature becomes lower than 273 K. A parameterization for precipitation is given in (A.8).

7. The shallow convection case: BOMEX

In this case data from the Barbados Oceanographic Meteorological Experiment (BOMEX) is used as input for the SUM. This data is used as the base of a LES comparison study (Siebesma, 2002). Hence the vertical profiles and especially the in-cloud vertical profiles of this case are well documented and can form good reference for the SUM output. The environmental profiles for θ and q_t are shown in figure 9.

Because KF is a moist convection scheme, it can only be applied above the LCL. For simplicity we assume the parcel to ascend adiabatically until the height at which KF applies, which is just above the LCL. As can be seen in figure 8 the environmental boundary layer is rather well mixed, so the error made due to this assumption is small.

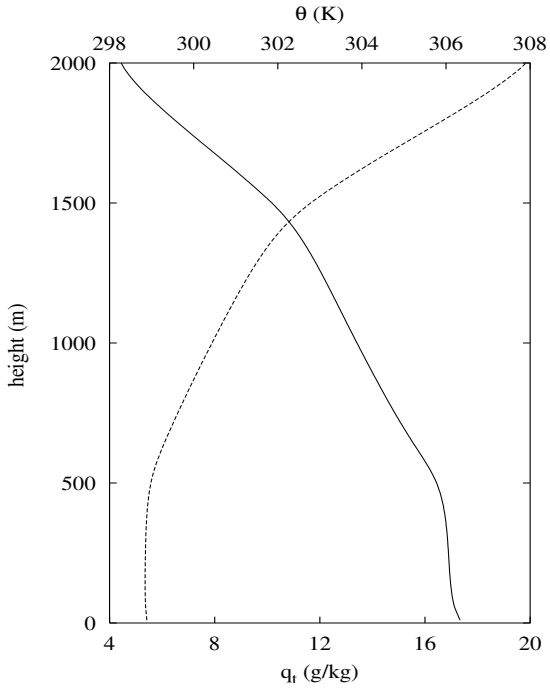

Figure 9. The vertical, environmental profiles for θ (dashed) and q_t, obtained by LES modeling. The cloud layer ranges from 500m to 1500m.

In 7.1 First SUM-results will be shown with preset ε and δ. This means that ε and δ are calculated without KF. These results can show whether the effort of the KF-scheme is in this case worthwhile. Next, result sets will be shown when ε and δ are calculated according to KF. It is assumed that the mixed parcels are Gaussian distributed. The fractional inflow rate ε_0 is varied and is either constant with height or proportional to the inverse of height.

7.1 Results

a)

Because ε and δ are preset, the profile of χ_c has no crucial meaning; therefore it will not be shown.

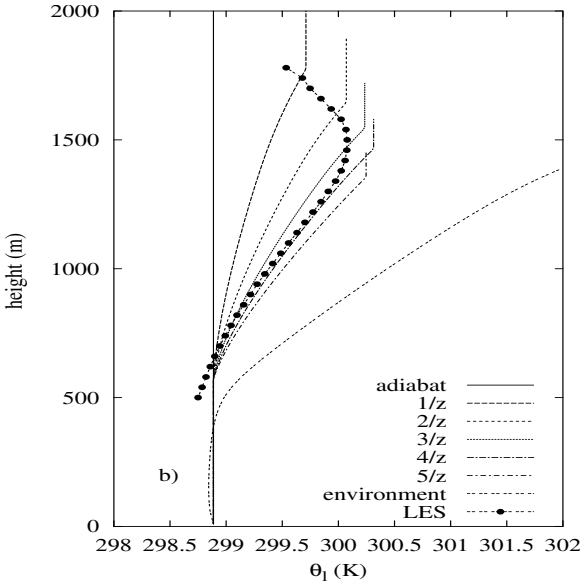

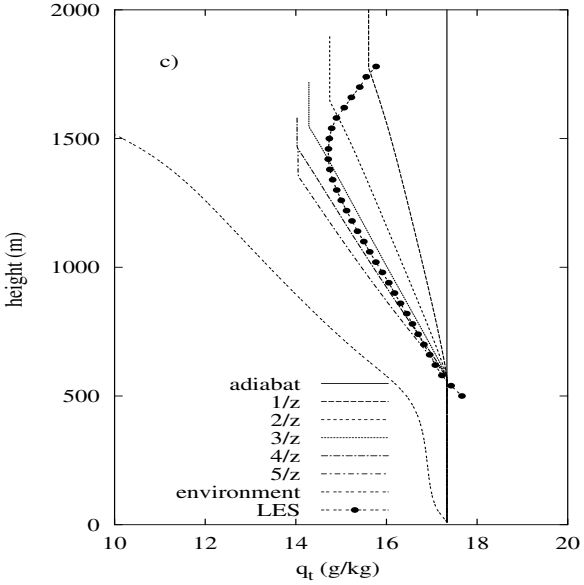

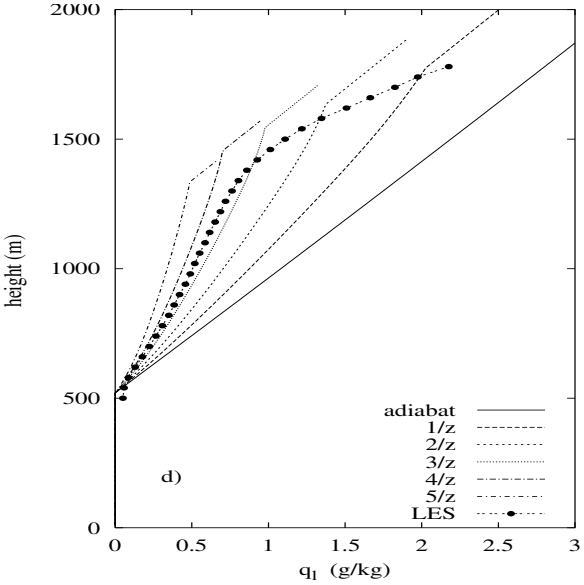

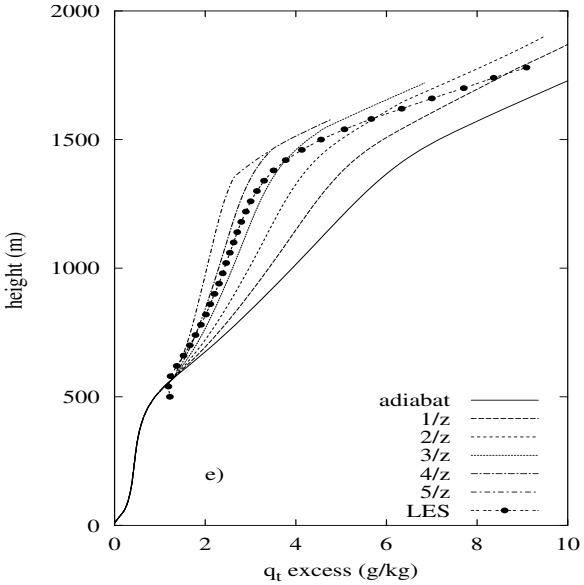

Figure 10. Updraft profiles with ε set to $0.3\frac{c}{z}$ and δ to $0.7\frac{c}{z}$ i.e. KF is switched off.

(a) χ_c, (b) liquid water potential temperature θ_l, (c) total water content q_t, (d) liquid water content q_l and (e) updraft excess in total water content The environmental, adiabatic and LES profiles are shown as well.

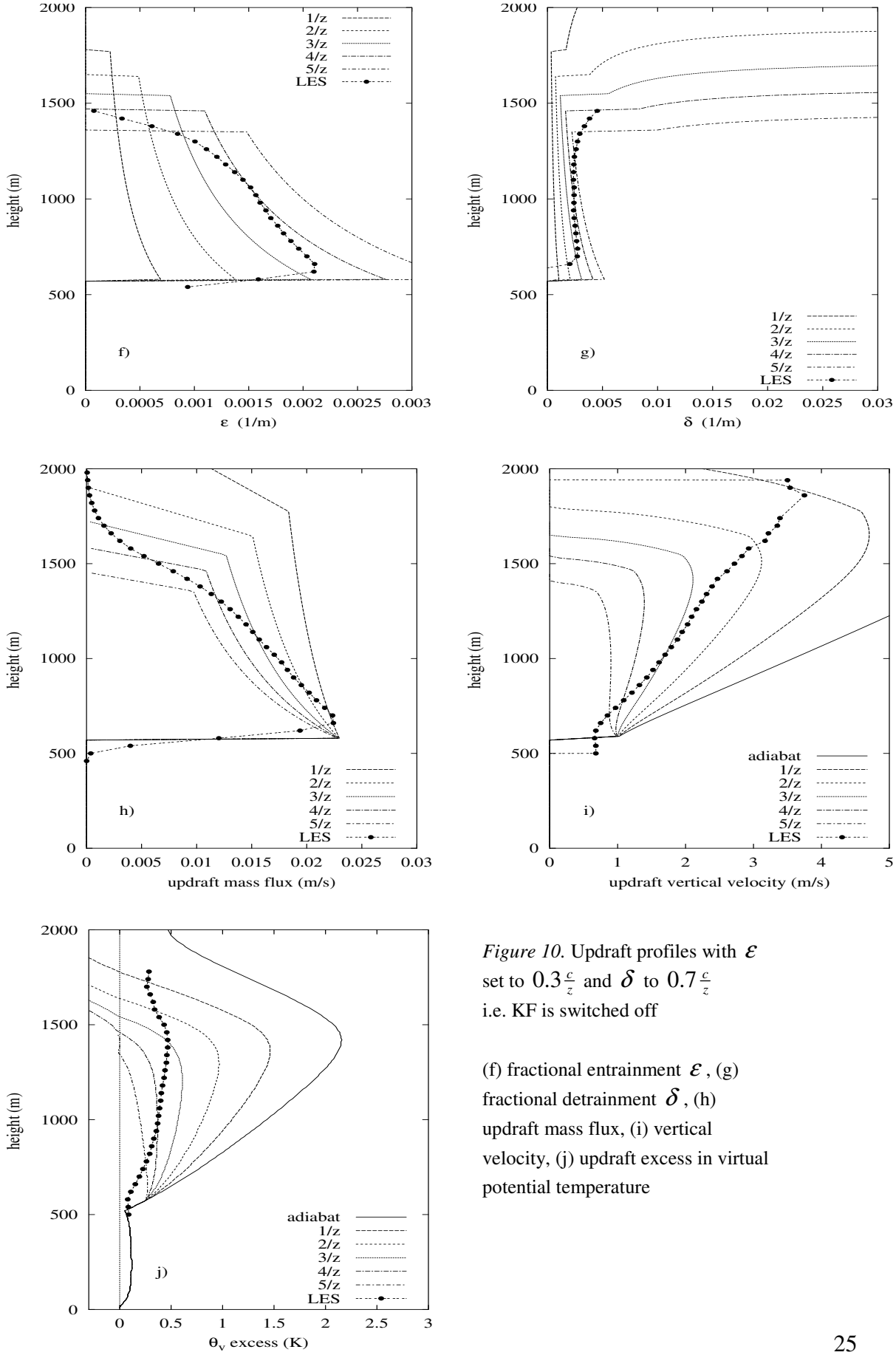

Figure 10. Updraft profiles with ε set to $0.3\frac{c}{z}$ and δ to $0.7\frac{c}{z}$ i.e. KF is switched off

(f) fractional entrainment ε, (g) fractional detrainment δ, (h) updraft mass flux, (i) vertical velocity, (j) updraft excess in virtual potential temperature

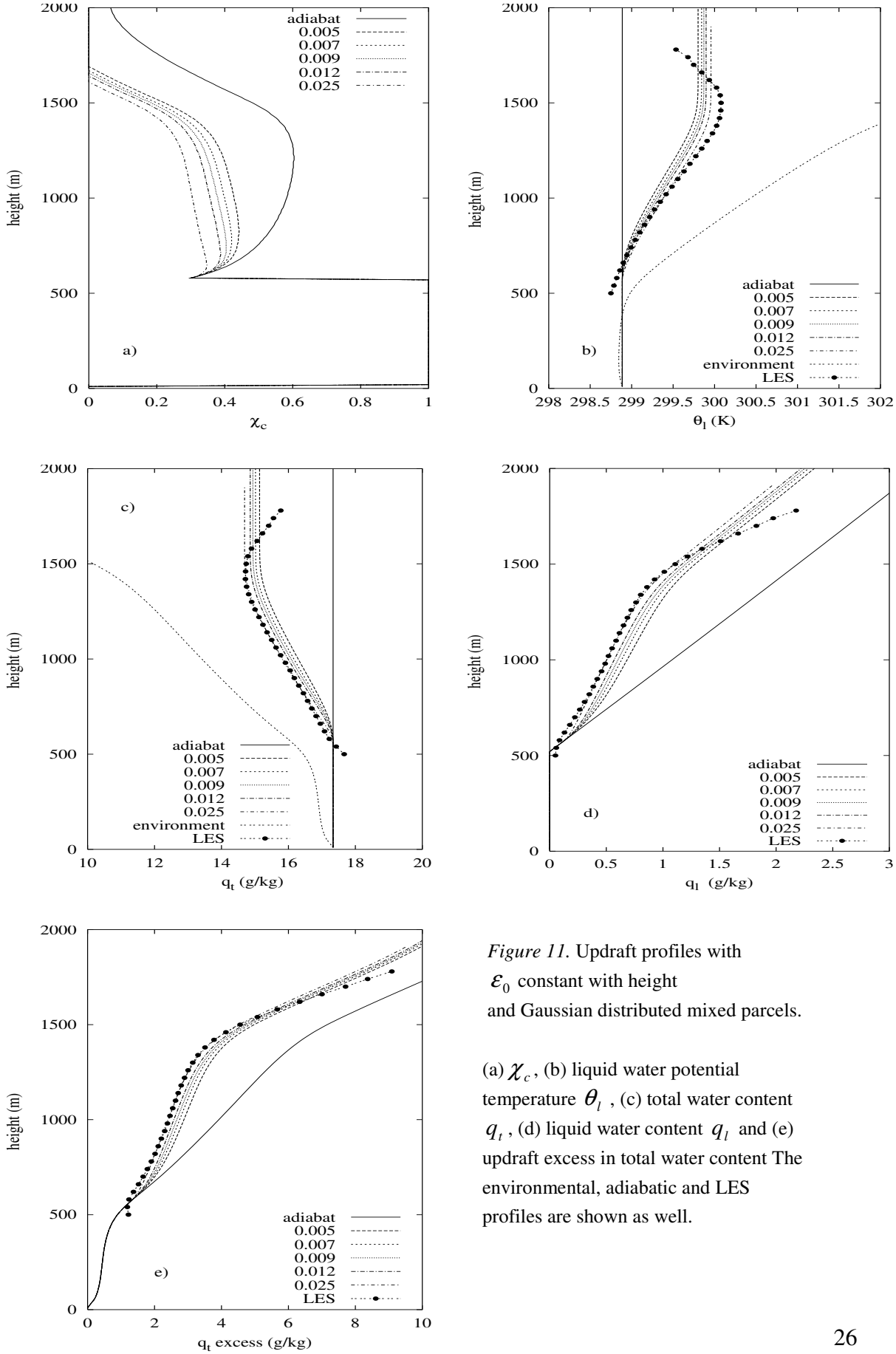

Figure 11. Updraft profiles with ε_0 constant with height and Gaussian distributed mixed parcels.

(a) χ_c, (b) liquid water potential temperature θ_l, (c) total water content q_t, (d) liquid water content q_l and (e) updraft excess in total water content The environmental, adiabatic and LES profiles are shown as well.

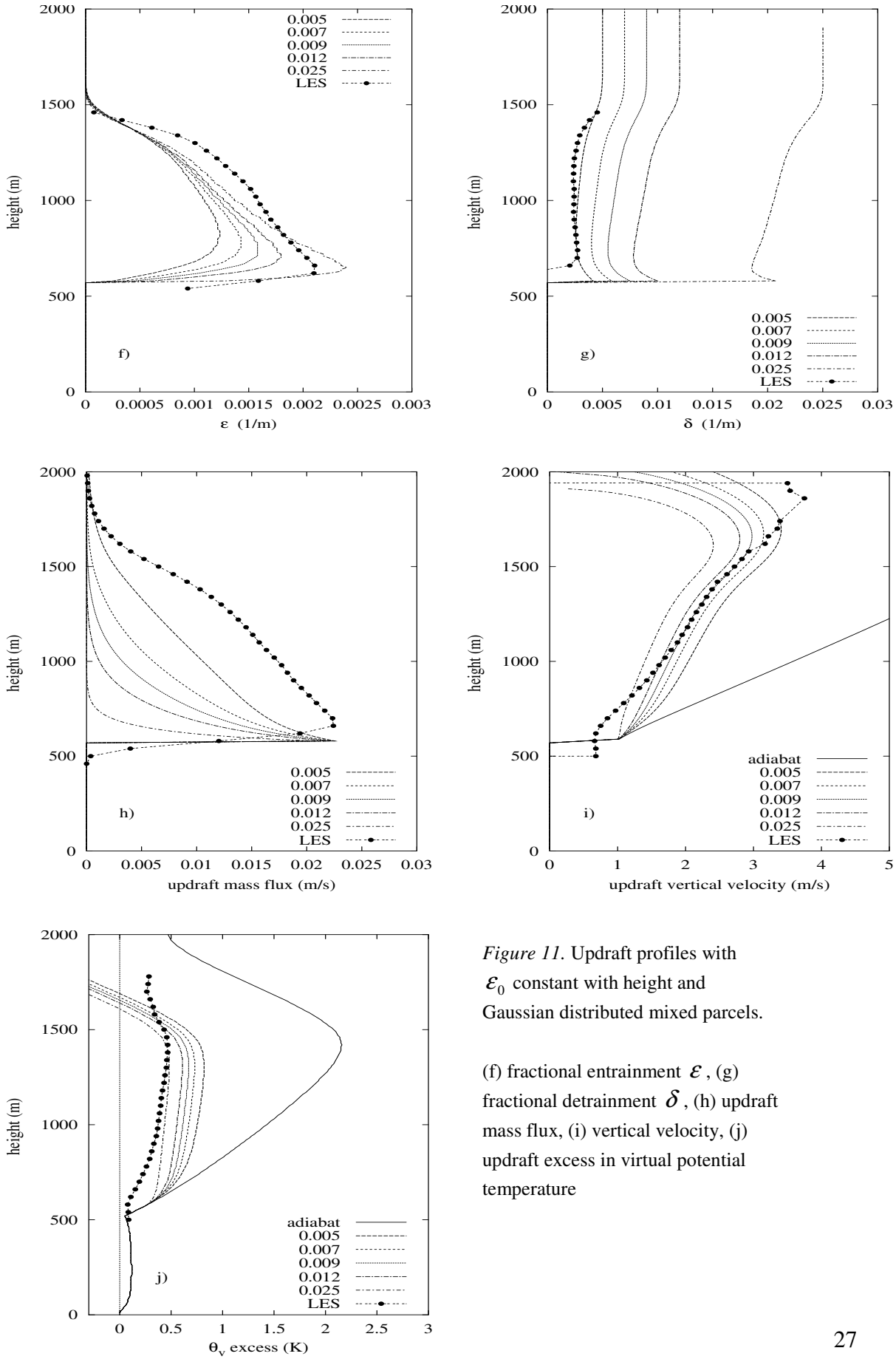

Figure 11. Updraft profiles with ε_0 constant with height and Gaussian distributed mixed parcels.

(f) fractional entrainment ε, (g) fractional detrainment δ, (h) updraft mass flux, (i) vertical velocity, (j) updraft excess in virtual potential temperature

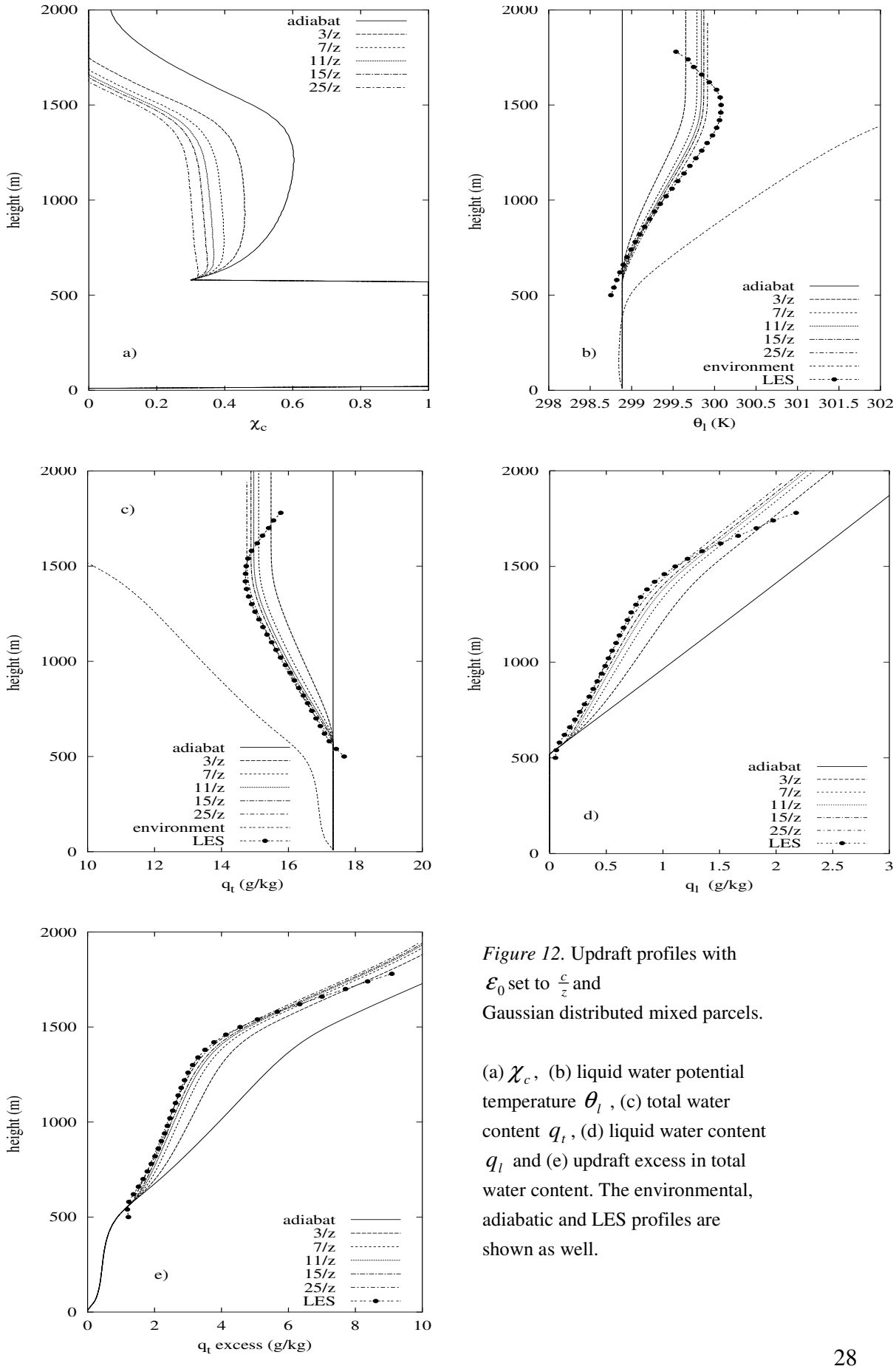

Figure 12. Updraft profiles with ε_0 set to $\frac{c}{z}$ and Gaussian distributed mixed parcels.

(a) χ_c, (b) liquid water potential temperature θ_l, (c) total water content q_t, (d) liquid water content q_l and (e) updraft excess in total water content. The environmental, adiabatic and LES profiles are shown as well.

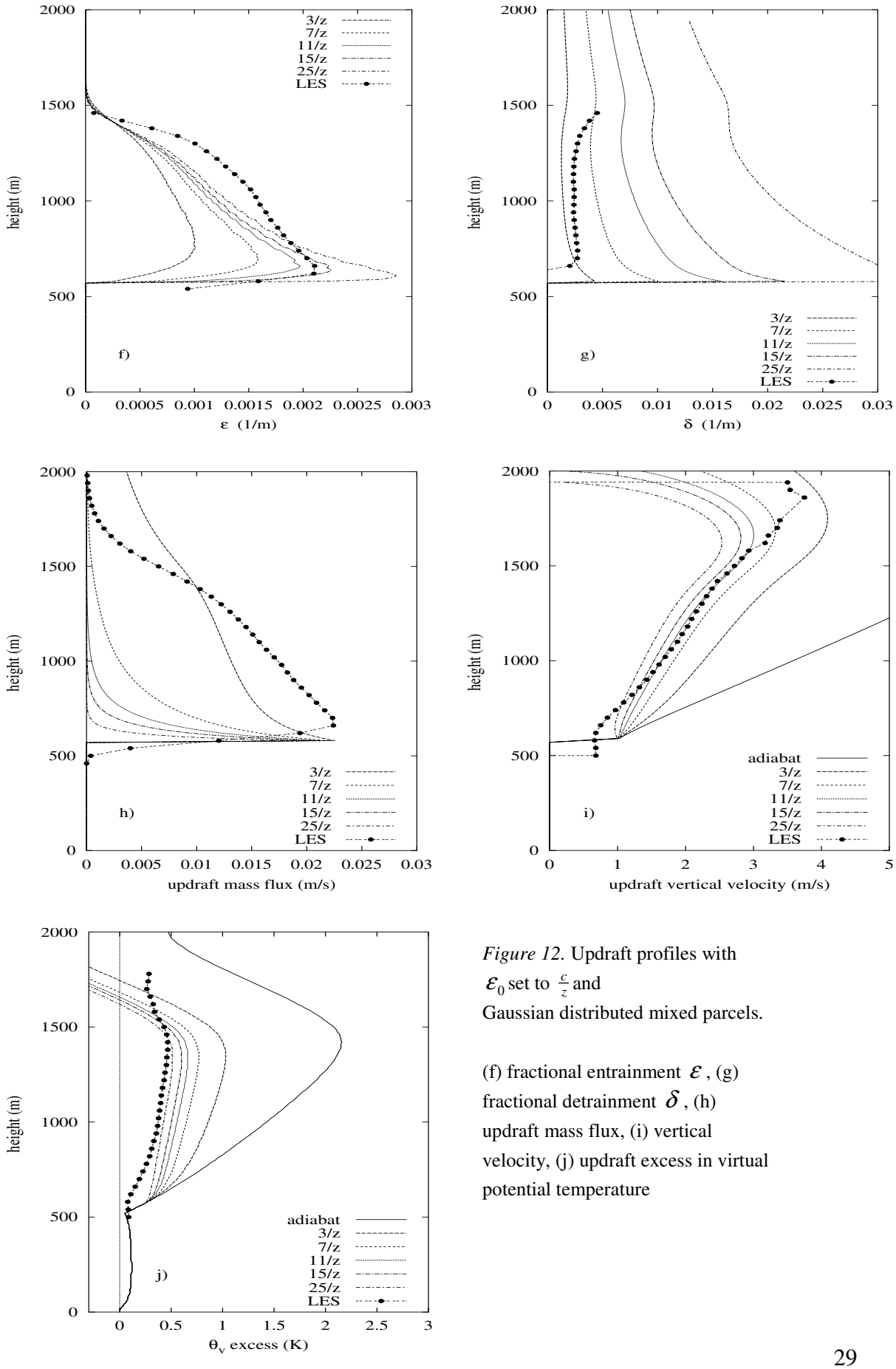

Figure 12. Updraft profiles with ε_0 set to $\frac{c}{z}$ and Gaussian distributed mixed parcels.

(f) fractional entrainment ε, (g) fractional detrainment δ, (h) updraft mass flux, (i) vertical velocity, (j) updraft excess in virtual potential temperature

7.2 Analysis

The SUM updraft properties ϕ are the result of the fractional entrainment ε, the environment of the cloud and the boundary values of ϕ. In this case ε_0 is the only varying parameter, so the differences between the updraft profiles for the three distinct result sets can be explained by examining the differences in ε_0.

First of all it is clear for each result set that the greater ε_0, the more the in cloud profiles for ϕ (and their derivatives) approach the environmental profile and the greater the difference with their adiabatic values.

In the KF-scheme the profile of ε is determined by the profile of χ_c and the distribution of the mixed parcels. The profile of χ_c shows for the distinct result sets the same qualitative behavior. Until just above the LCL χ_c is equal to one. This means that the ascending parcel has positive excess in θ_v in the whole sub-cloud layer. This is not in agreement with the profiles given in figure 4 that suggest that a parcel is - in general - negatively buoyant just above the LCL. This is caused by the light decrease with height of $\overline{q_t}$, as can be seen in e.g. figure 10c. The decrease of $\overline{q_t}$ causes $\overline{\theta_v}$ to decrease with height as well. This causes the adiabatic ascending parcel to be positively buoyant in the whole sub-cloud layer.Because the parcel is unsaturated as long as it is under its LCL, evaporative cooling is zero and hence χ_c is equal to one. When the evaporative cooling is sufficient to form negative buoyant mixed parcels as well, χ_c becomes smaller than one.

The profile of χ_c above the LCL is dependent on ε_0. When, at a given height, all other variables are kept equal, the value of χ_c is not dependent on the value of ε_0. However, at that height ε is still dependent on ε_0; the smaller ε_0, the smaller ε and vice versa. The magnitude of ε at a given height dictates together with the updraft excess in ϕ the vertical gradient in ϕ. This makes the profile of χ_c and thus the profile of ε and hence all other profiles dependent on ε_0. An increase in ε_0 yields as can be seen in e.g. figure 11a and 12a a smaller χ_c. If it was not for the mass flux and fractional detrainment profile, one could conclude that values of ε_0 around 0.025 m^{-1} or $25/z$ make the SUM with Gaussian distributed mixed parcels capable of reproducing the LES results. However, the fractional detrainment profiles for both ε_0 constant with height and ε_0 proportional to the inverse of height are too large with these values for ε_0. This encourages the use of another PDF for the mixed parcels. A homogeneous distribution of the mixed parcels will not provide a solution for this problem; it will only decrease both ε and δ, as can be seen in figure 7.

When the asymmetric PDF is applied instead of the Gaussian PDF (or any symmetric PDF), this yields for a given ε_0 and χ_c to a larger entrainment and smaller detrainment as can be seen in figures A.2 and 7. This can be understood by examining the amount of mixed parcels that is entrained / detrained. When the mixed parcels are asymmetrically distributed like in figure A.2, this means that the ensemble mixed parcels consists of

more parcels with a low fraction of environmental air and therefore less parcels with a high fraction of environmental air. Given a χ_c, the amount of parcels with χ greater than χ_c is therefore smaller and therefore the amount of parcels that detrains is smaller as well. Thus, when we apply the asymmetric PDF, this could lead to the right profiles for both ε and δ. Because it can be diagnosed from LES results (Siebesma, 2002) that ε_0 is proportional to the inverse of height and because it is suggested by figure 10 that the SUM without KF works quite good when ε_0 is set this way, we now investigate (figure 13) some updraft profiles with asymmetric distributed mixed parcels and ε_0 proportional to the inverse of height.

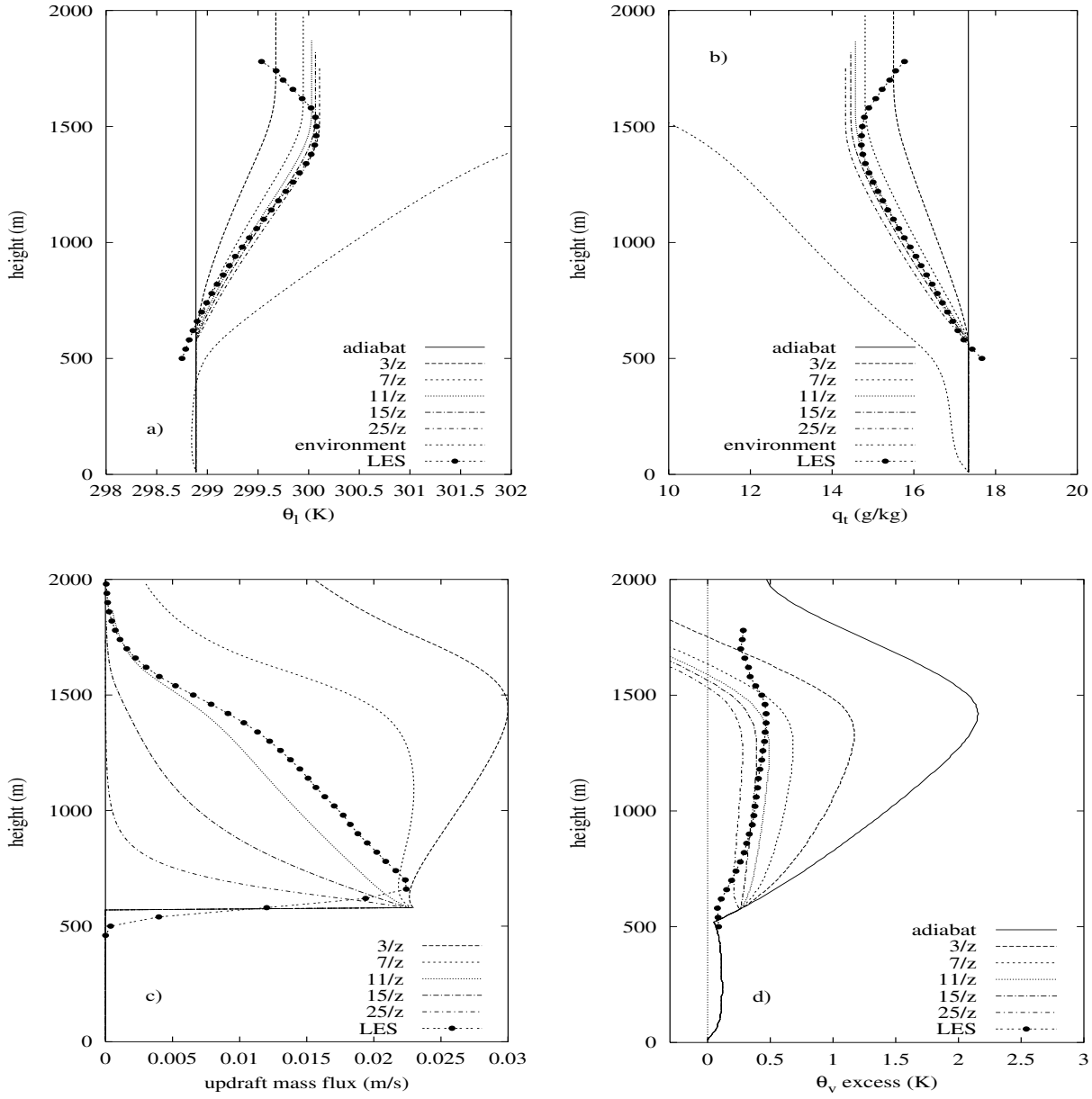

Figure 13. Updraft profiles with ε_0 set to $\frac{c}{z}$ and asymmetrically distributed mixed parcels. (a) liquid water potential temperature θ_l, (b) total water content q_t, (c) updraft mass flux and (d) excess in updraft virtual potential temperature.

It can be concluded from figure 13 that the SUM with asymmetrically distributed mixed parcels, together with ε_0 proportional to the inverse of height resembles the LES results rather well. In order to elucidate the impact of the mixed parcel distribution some more, updraft profiles with $\varepsilon_0 = 11/z$ and distinct distributions are plotted in figure 14.

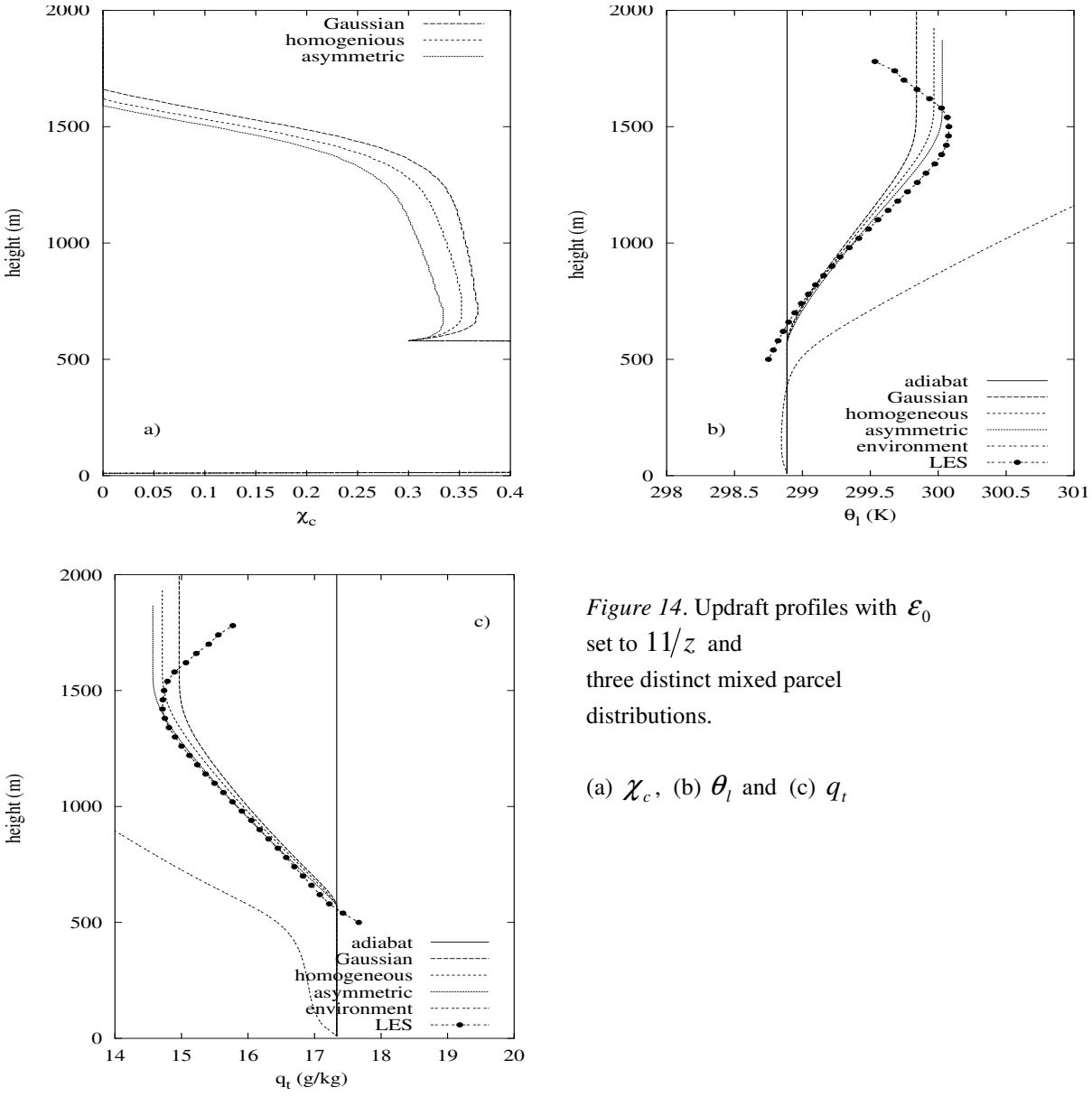

Figure 14. Updraft profiles with ε_0 set to $11/z$ and three distinct mixed parcel distributions.

(a) χ_c, (b) θ_l and (c) q_t

The profiles in figure 14 show that the PDF has no substantial influence on the updraft profiles for ϕ. This can be understood when we examine figure 7 once more. As can be seen in figure 14a, typical values for χ_c are around 0.35. In figure 7 it is clear that for these values of χ_c (for lower values as well) ε is hardly dependent on the considering PDF. This is a consequence of the low amount of environmental air in the mixed parcels that have a low value for χ.

Because the updraft profiles for ϕ are determined by the profile of ε, the profiles of χ_c and ϕ are not rather distinct. As can be seen (figures 7 and 14g) the fractional detrainment actually is substantially influenced by the PDF. When the asymmetric PDF is considered, the fractional entrainment is hardly different compared to the symmetric PDF; whereas the fractional detrainment is substantially lower. Because the fractional detrainment does not influence the updraft profiles, the asymmetric PDF improves in this case the performance of the KF-scheme.

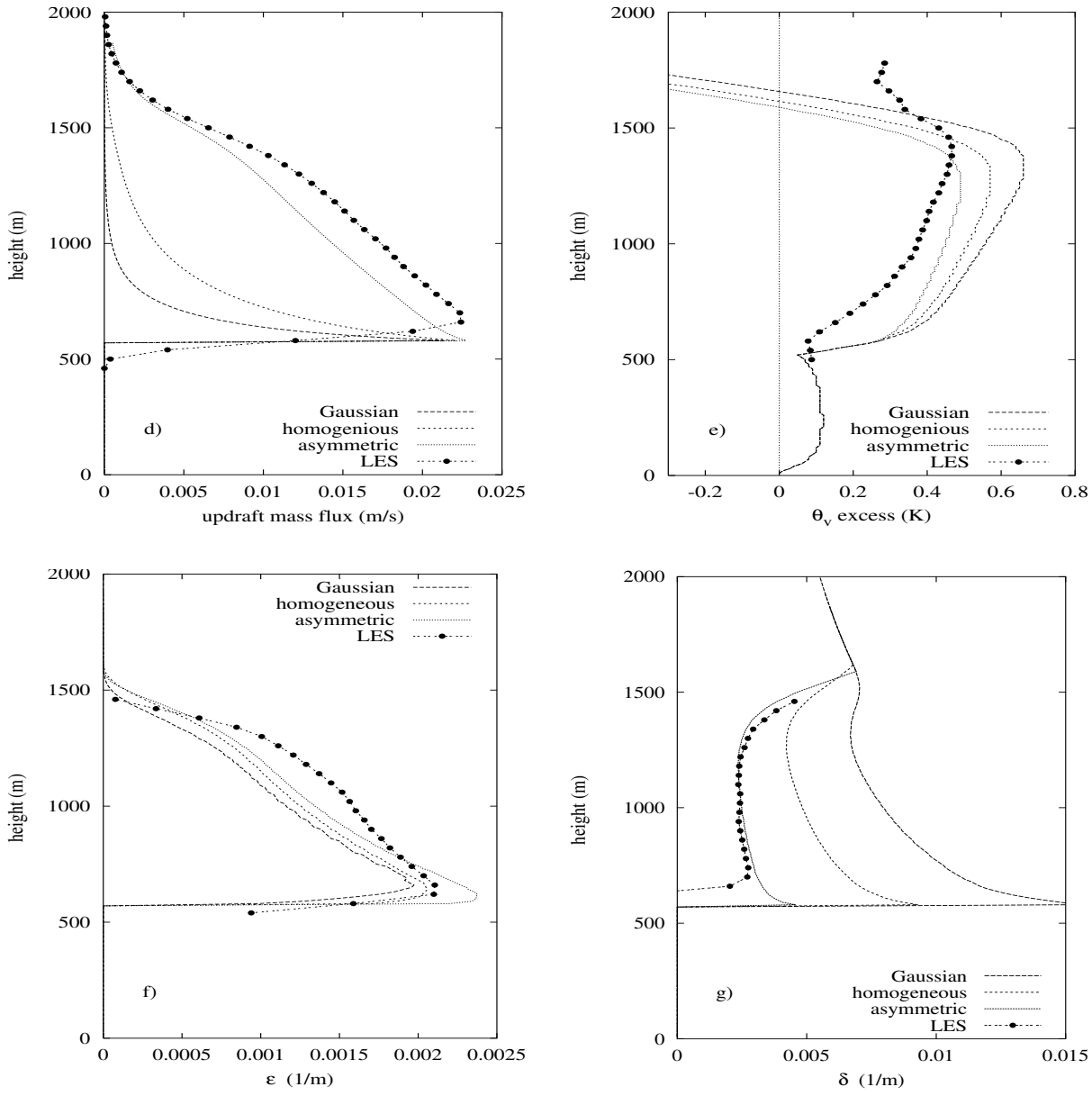

Figure 14. Updraft profiles with ε_0 set to $11/z$ and three distinct mixed parcel distributions.
(d) updraft excess in virtual potential temperature, (e) updraft mass flux,
(f) fractional entrainment ε and (g) fractional detrainment δ.

8. Sensitivity to relative humidity

The first question that needs answering is how χ_c depends on the variation of the relative humidity. This dependency is depicted in figure 15.

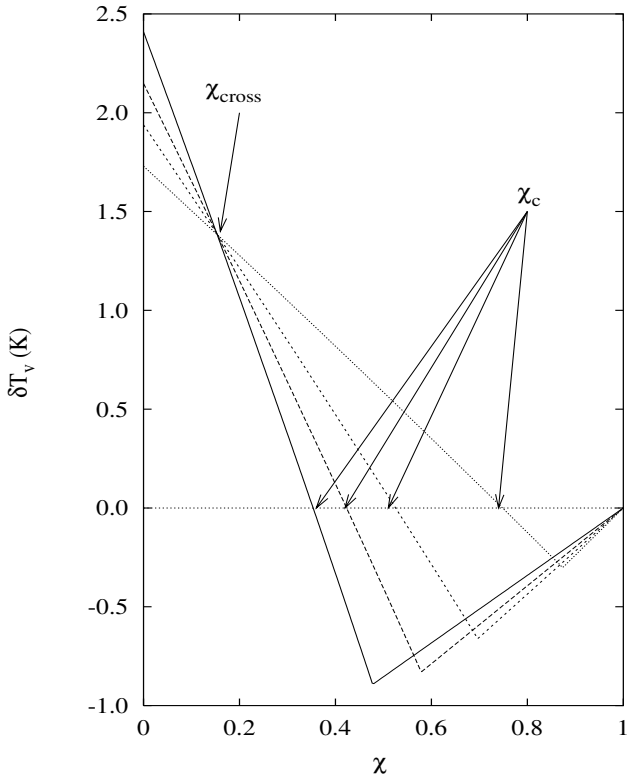

Figure 15. Difference between the mixed parcel virtual temperature and environmental virtual temperature for RH = 25 % (solid), RH=50% (long dashed), RH=70% (short dashed) and RH=90% (dotted). The other ambient conditions are similar to that of Figure 5.

When the relative humidity increases, χ_c increases. This is a bit remarkable, because the virtual potential temperature of the environment increases when its relative humidity increases, so the difference in virtual potential temperature between the pure cloudy air and the environment decreases. This can be seen in Figure 15. This decrease leads not to a decrease of χ_c, because the evaporative cooling is less strong when the relative humidity is high, which makes δT_v to fall less rapid as χ increases. This leads in the end to a higher χ_c. The value of χ at which the distinct lines of δT_v intersect is depicted as χ_{cross} (A.6).

Variation of q_l and temperature difference between cloud and environment influence χ_c as well. A summary of the correlation between χ_c and the distinct variables is given next in figure 16.

RH	+	A higher RH leads to less evaporative cooling
q_l	-	A higher liquid water content decreases the in-cloud T_v and hence δT_v
δT	+	A higher δT yields a higher δT_v

Figure 16. The plus or minus sign depicts the correlation between the change in the variable and χ_c, δT is the difference in temperature between the cloud and its environment.

The relative humidity sensitivity test is performed with the profiles shown in figure 17. The only profile that is varied is the relative humidity profile, and hence the q_t profile. The initial relative humidity profiles were constant with height above 2 km (Derbyshire, 2003). The profiles that are used in the test are 12-hourly averaged CRM profiles. The relative humidity varies with height due to convective activity, but this does not influence the sensitivity test.

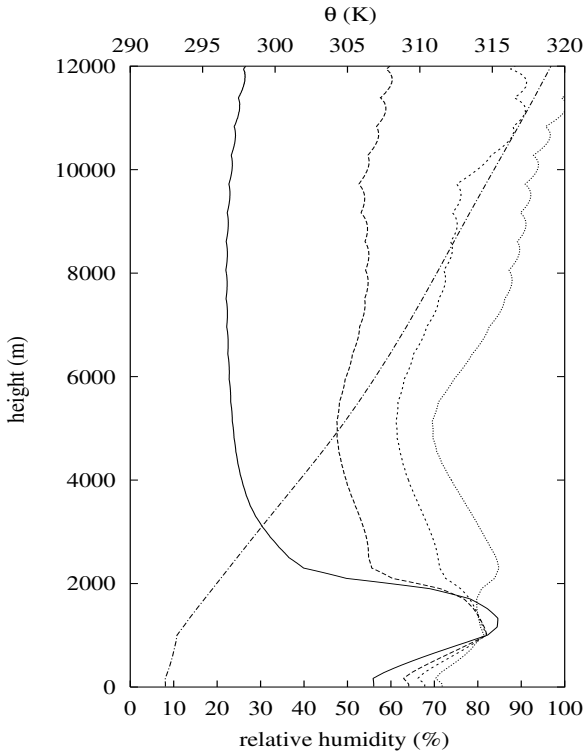

Figure 17. The environmental mean profiles for the sensitivity test. The profiles are varied in relative humidity only. The relative humidity is defined as the ratio of q_v and q_s.

8.1 Results

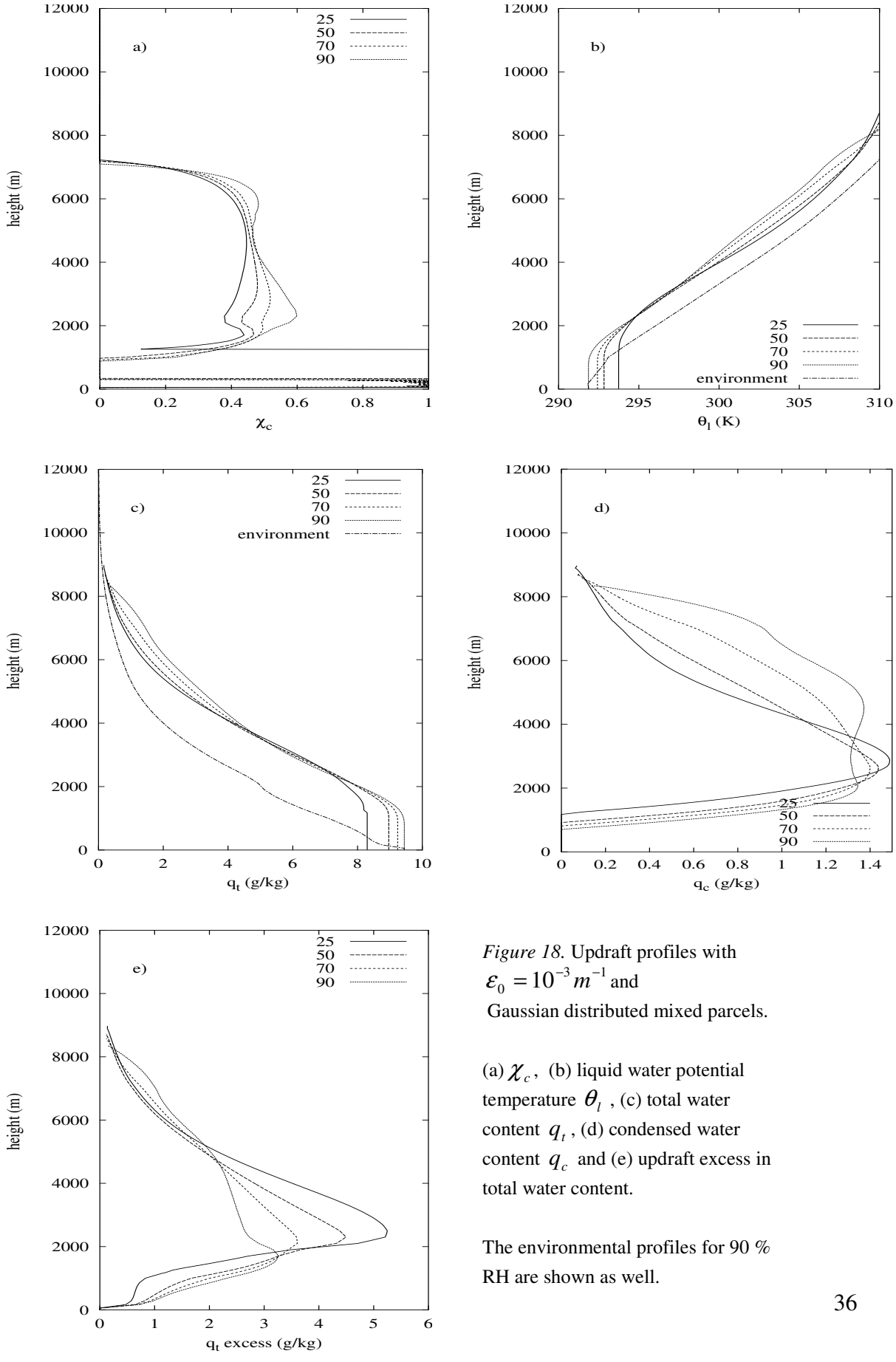

Figure 18. Updraft profiles with $\varepsilon_0 = 10^{-3}\, m^{-1}$ and Gaussian distributed mixed parcels.

(a) χ_c, (b) liquid water potential temperature θ_l, (c) total water content q_t, (d) condensed water content q_c and (e) updraft excess in total water content.

The environmental profiles for 90 % RH are shown as well.

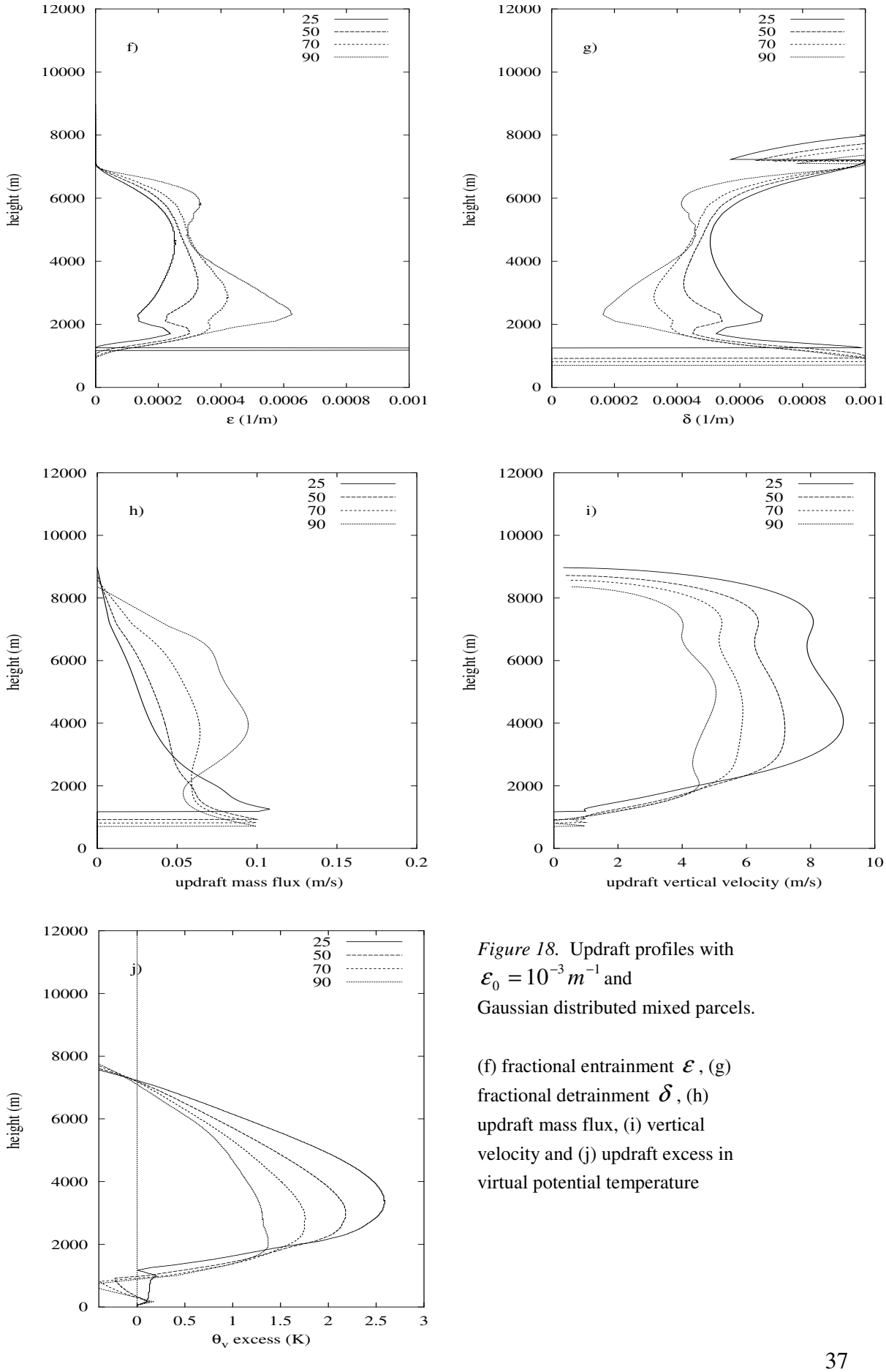

Figure 18. Updraft profiles with $\varepsilon_0 = 10^{-3} m^{-1}$ and Gaussian distributed mixed parcels.

(f) fractional entrainment ε, (g) fractional detrainment δ, (h) updraft mass flux, (i) vertical velocity and (j) updraft excess in virtual potential temperature

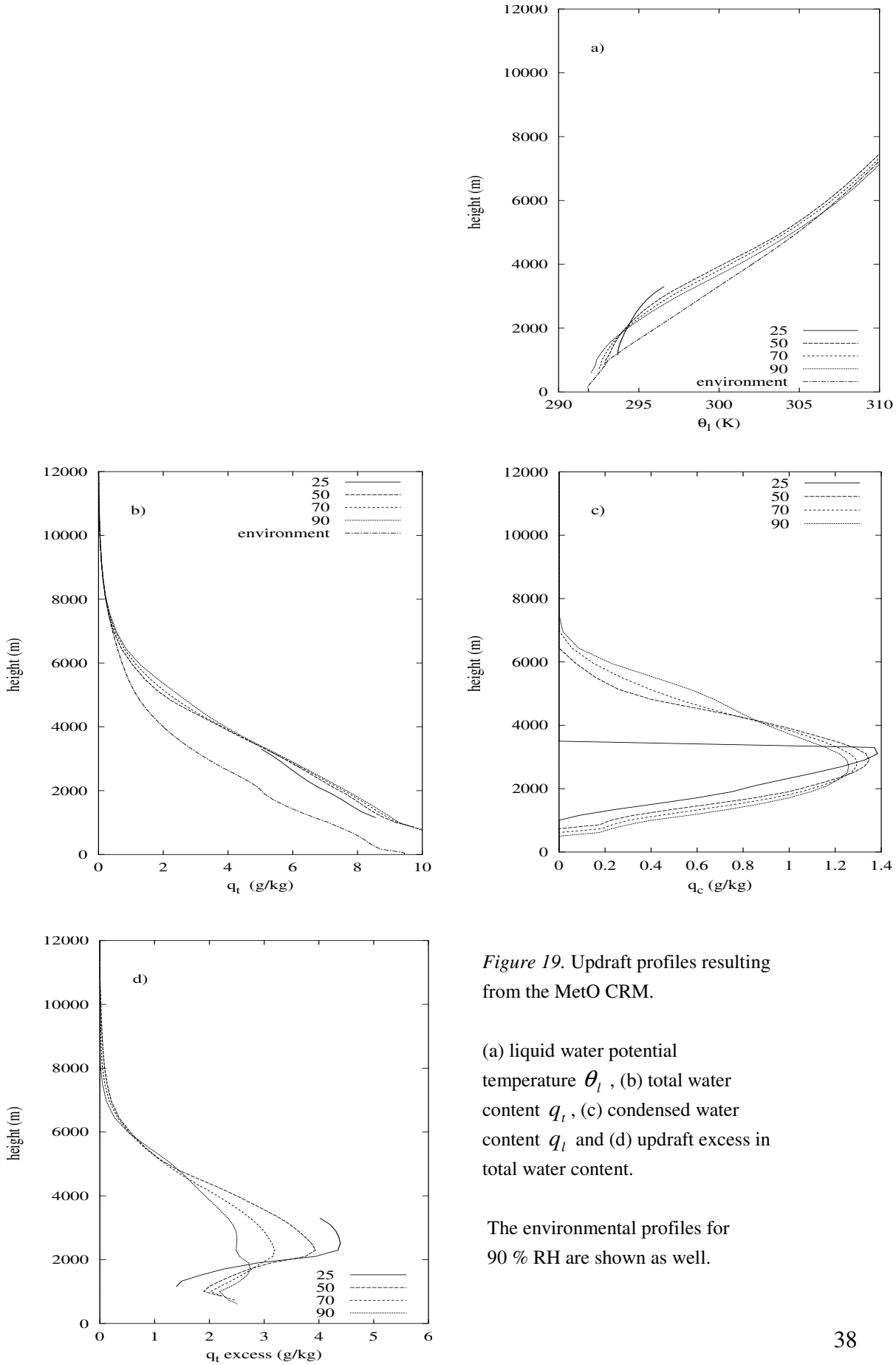

Figure 19. Updraft profiles resulting from the MetO CRM.

(a) liquid water potential temperature θ_l , (b) total water content q_t , (c) condensed water content q_l and (d) updraft excess in total water content.

The environmental profiles for 90 % RH are shown as well.

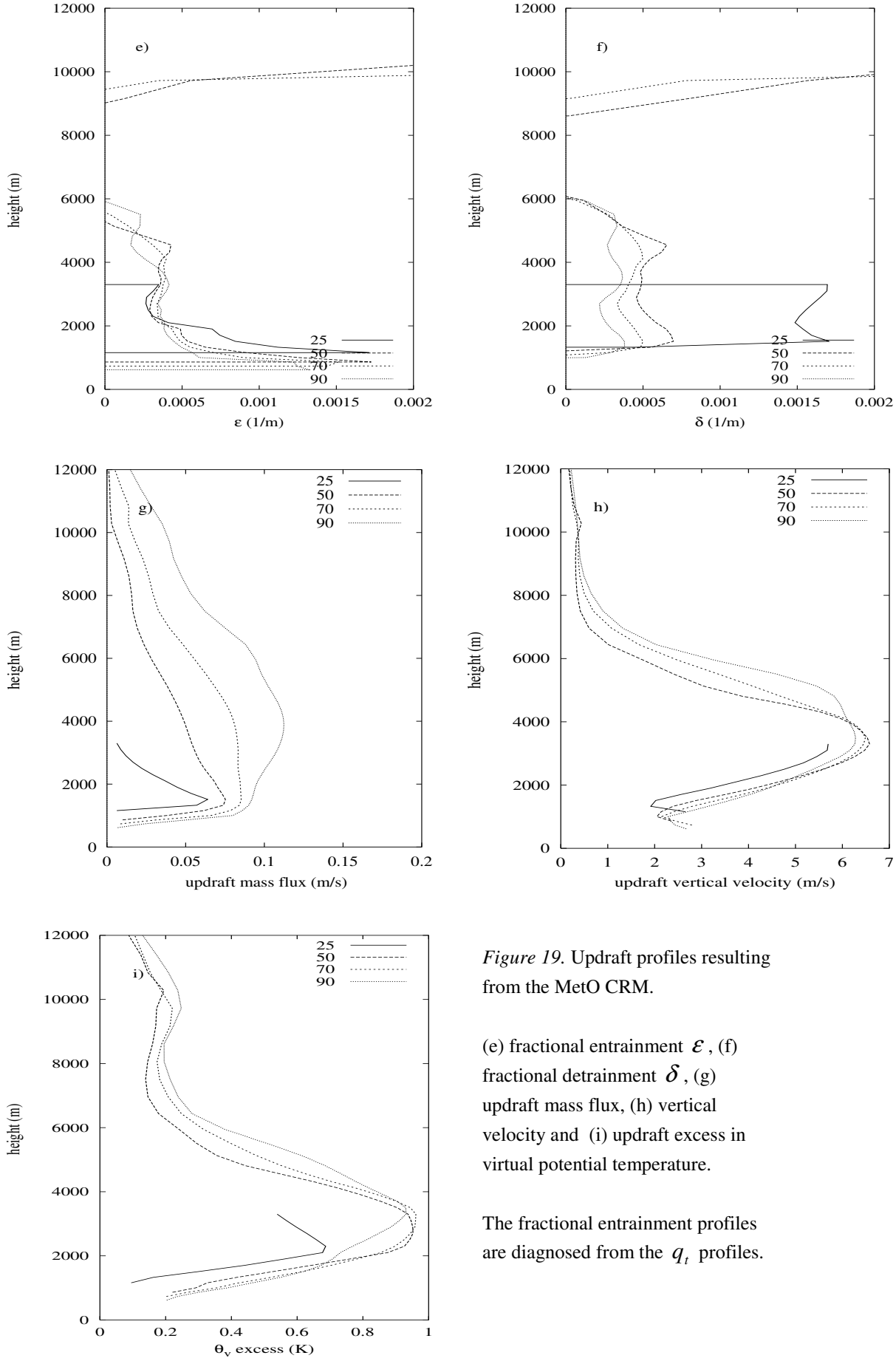

Figure 19. Updraft profiles resulting from the MetO CRM.

(e) fractional entrainment ε, (f) fractional detrainment δ, (g) updraft mass flux, (h) vertical velocity and (i) updraft excess in virtual potential temperature.

The fractional entrainment profiles are diagnosed from the q_t profiles.

a)

Because ε and δ are preset, the profile of χ_c has no crucial meaning; therefore it will not be shown.

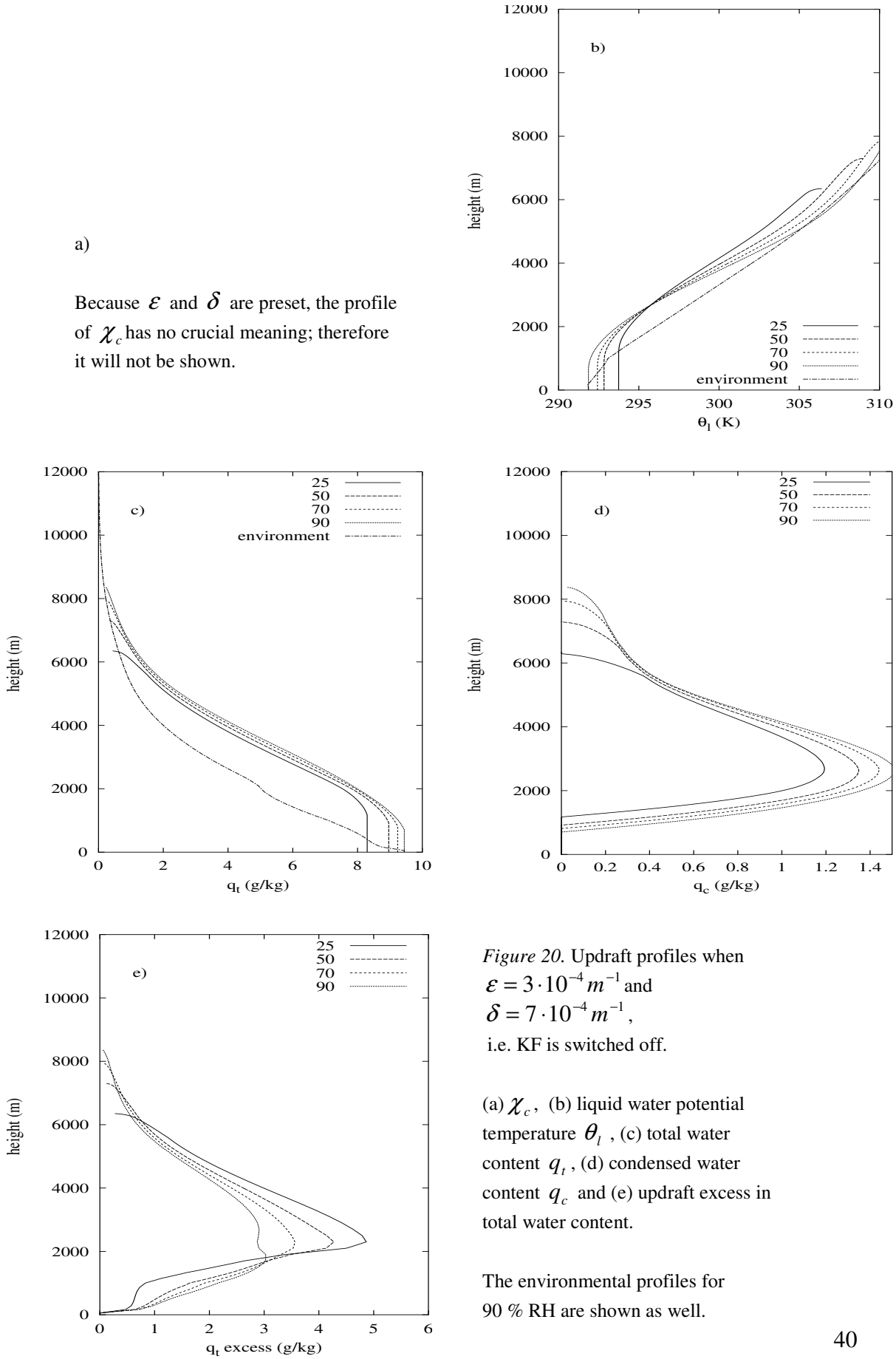

Figure 20. Updraft profiles when $\varepsilon = 3 \cdot 10^{-4} m^{-1}$ and $\delta = 7 \cdot 10^{-4} m^{-1}$, i.e. KF is switched off.

(a) χ_c, (b) liquid water potential temperature θ_l, (c) total water content q_t, (d) condensed water content q_c and (e) updraft excess in total water content.

The environmental profiles for 90 % RH are shown as well.

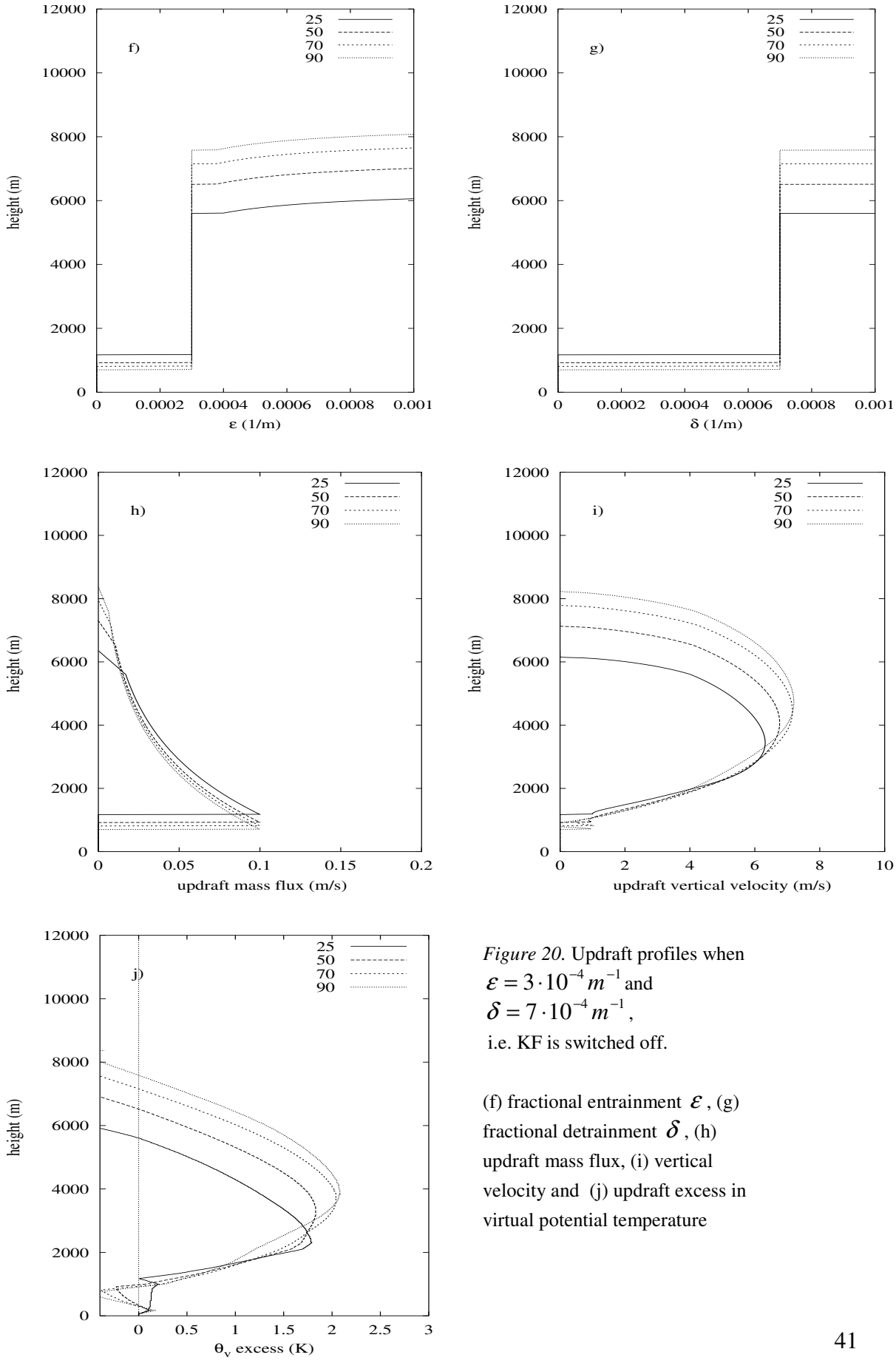

Figure 20. Updraft profiles when $\varepsilon = 3 \cdot 10^{-4} m^{-1}$ and $\delta = 7 \cdot 10^{-4} m^{-1}$, i.e. KF is switched off.

(f) fractional entrainment ε, (g) fractional detrainment δ, (h) updraft mass flux, (i) vertical velocity and (j) updraft excess in virtual potential temperature

8.2 Analysis

When we want to compare the SUM results to the CRM results it should be stressed in the first place that unlike the shallow cumulus case results the quantitative resemblance is rather poor. As can be seen in figure 18, the sensitivity of the KF-scheme to the relative humidity, that is to be tested in the first place, is wrong.
The first discrepancy one encounters is in the depth of the cloud layer. In the SUM this depth is best represented as the height interval in which the vertical velocity has a positive value. The CRM shows that a lower relative humidity yields a smaller cloud depth, or lower cloud top. The SUM cloud top reacts the other way around to relative humidity, i.e. a lower relative humidity yields a higher cloud top.

In this test it is ε together with the environment that determines the updraft profiles, whereas in the shallow cumulus case it was just ε. The dependency of the updraft profiles on ε_0 is the same in this case as it is in the case of shallow cumulus. Therefore ε_0 is not varied in this test and is set constant with height.

So, the KF cloud top problem can be explained in terms of the relative humidity and the profile of χ_c. In figure 15 it is shown that if the relative humidity decreases, χ_c decreases as well. This effect is visible in figure 18a. For almost the whole depth of the cloud χ_c is smaller when the environment of the cloud is dryer, but the spacing between the distinct profiles decreases with height and - eventually - at around 7000m the profiles intersect. The decrease in spacing and the intersection of the distinct χ_c profiles is caused by the different dilution of the updrafts. The dilution is represented by the term on the RHS of (12) and is the product of minus the fractional entrainment and the cloud excess in ϕ. In the shallow cumulus case it was shown that a lower fractional entrainment yields a higher cloud top. Because the profiles for $\bar{\phi}$ were not varied in that case, one can as well state that a lower dilution yields a higher cloud top. Analogous, the vertically averaged dilution - when KF is concerned - has less impact when the relative humidity is lower. This explains the decrease is spacing between the χ_c profiles, the intersection and the cloud top problem. It explains as well why the sensitivity of the profiles of ϕ_c is not in agreement with the CRM-results. When e.g. the $\theta_{l,c}$-profiles (figures 18b and 20b) are compared, it can be seen that the sensitivity of the SUM profile is opposite to the sensitivity of the CRM-profile. Because the $\bar{\theta}_l$-profile is not varied in this test, the wrong sensitivity can - according to (12) - only be explained by wrong sensitivity of ε. When figures 18f and 20e are compared it can be concluded that the SUM indeed adapts ε wrong.

The wrong sensitivity is even clearer when the θ_v-excess profiles are compared (figures 18j, 19i and 20j). And however $\overline{\theta_v}$ is a function of the relative humidity, the same argument as with the $\overline{\theta_l}$-profile can be used to explain.

Unlike in the previous, shallow convection case modifications to the inflow rate and mixed parcel PDF will not provide a solution for this problem, because χ_c decreases when the relative humidity decreases. Any mixed parcel PDF will result in a smaller ε when χ_c decreases. When the fractional inflow rate - like in the previous case - is set proportional to the inverse of height, the wrong sensitivity will not be improved either. Again the solution fails because of the behavior of χ_c.
The wrong sensitivity of ε can be partially improved when χ_c is neglected; i.e. by making ε and δ independent of χ_c. In figure 20 the results of the SUM with ε and δ preset to a constant value are shown. The jumps in ε and δ at around 6 km are caused by the enhanced inflow rate between the LZB and the cloud top (see A.8). This enhanced inflow rate causes the mass flux above the LZB to decrease linearly with height in order to become zero at the cloud top. This is more a model artifact than a phenomenon with physical reasons.
With preset values for ε and δ, the sensitivity - including the height of the cloud top - is in better agreement with the CRM results. But, presetting ε and δ makes - as expected - the mass flux insensitive to the relative humidity (figure 20h), which is highly unwanted in this very study. This insensitivity can be solved when we use the feature of (12) that states that ϕ_c is independent on δ. This encourages the use of a preset ε and a χ_c-dependent δ. When the KF-scheme is modified this way, the cloud properties ϕ_c, as well as the mass flux will be sensitive (to the relative humidity) in the good direction. In figure 20a schematic illustration of the modified KF-scheme is given. Results of the SUM with this modification to the KF-scheme are shown in figure 21. This modification to the scheme is discussed more extensively in A.7.

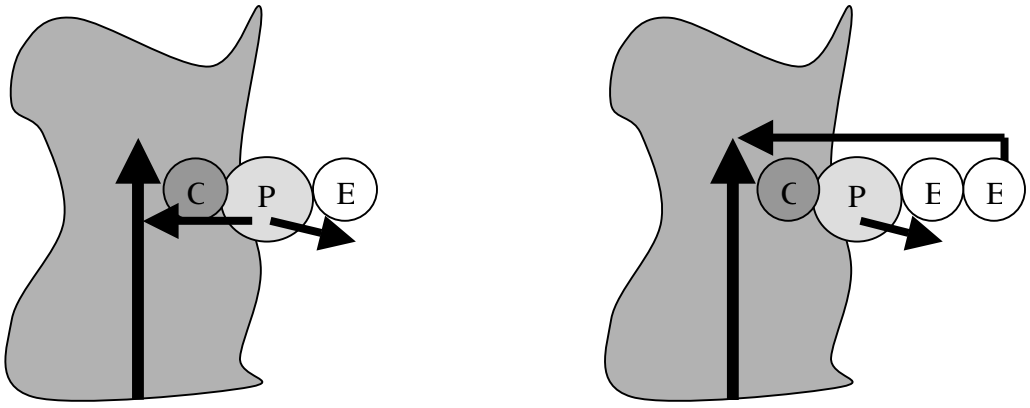

Figure 20. **Left:** the standard KF-scheme: ε and δ are both determined from the properties of the mixed parcels at the periphery P of the cloud. **Right:** the modified KF-scheme: δ is determined from the properties of the mixed parcels whereas ε is independent from these properties. Therefore, the under determination of ε is omitted. Environmental parcels are depicted with e, cloudy parcels with c.

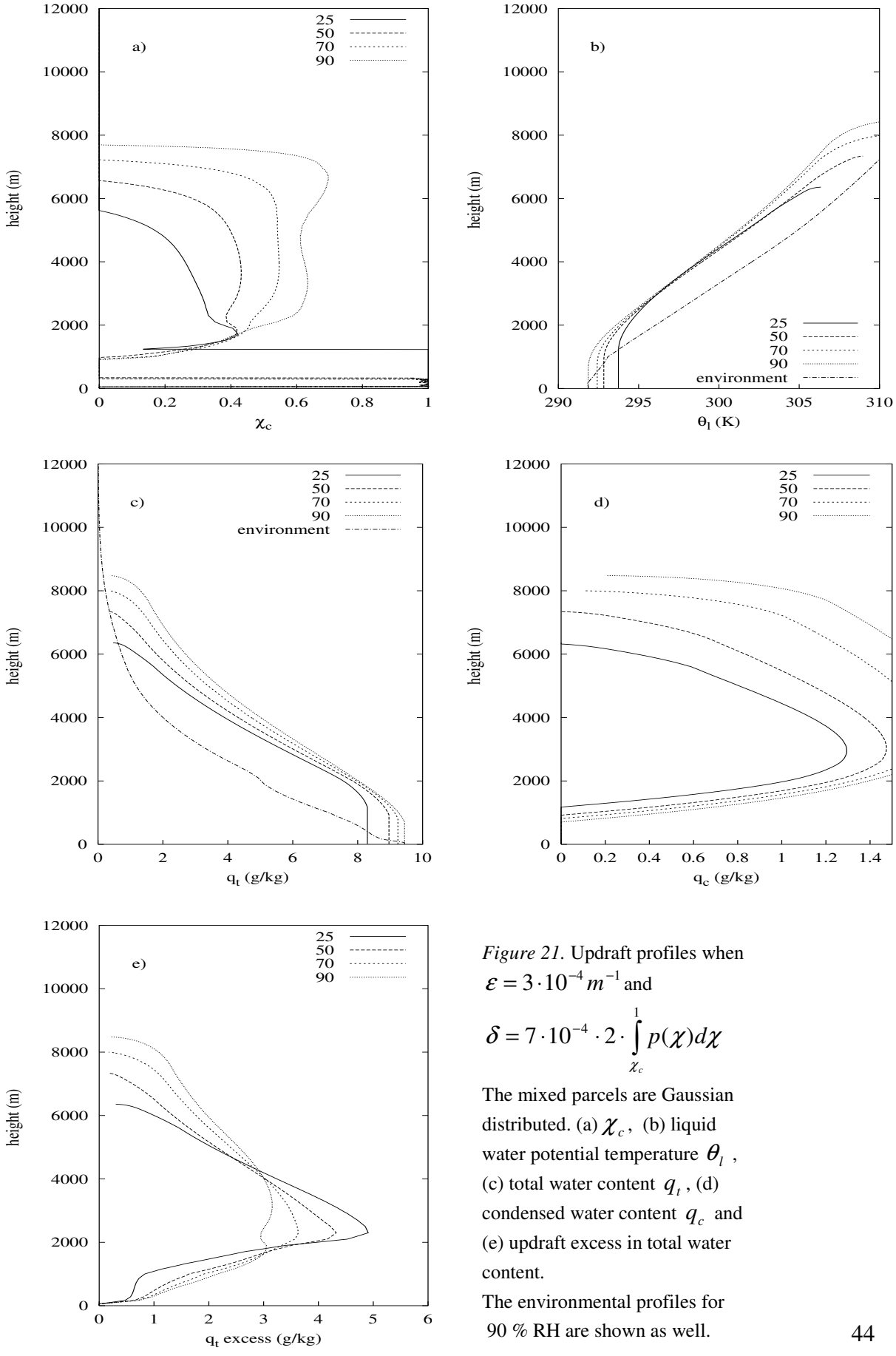

Figure 21. Updraft profiles when $\varepsilon = 3 \cdot 10^{-4} m^{-1}$ and

$$\delta = 7 \cdot 10^{-4} \cdot 2 \cdot \int_{\chi_c}^{1} p(\chi) d\chi$$

The mixed parcels are Gaussian distributed. (a) χ_c, (b) liquid water potential temperature θ_l, (c) total water content q_t, (d) condensed water content q_c and (e) updraft excess in total water content.
The environmental profiles for 90 % RH are shown as well.

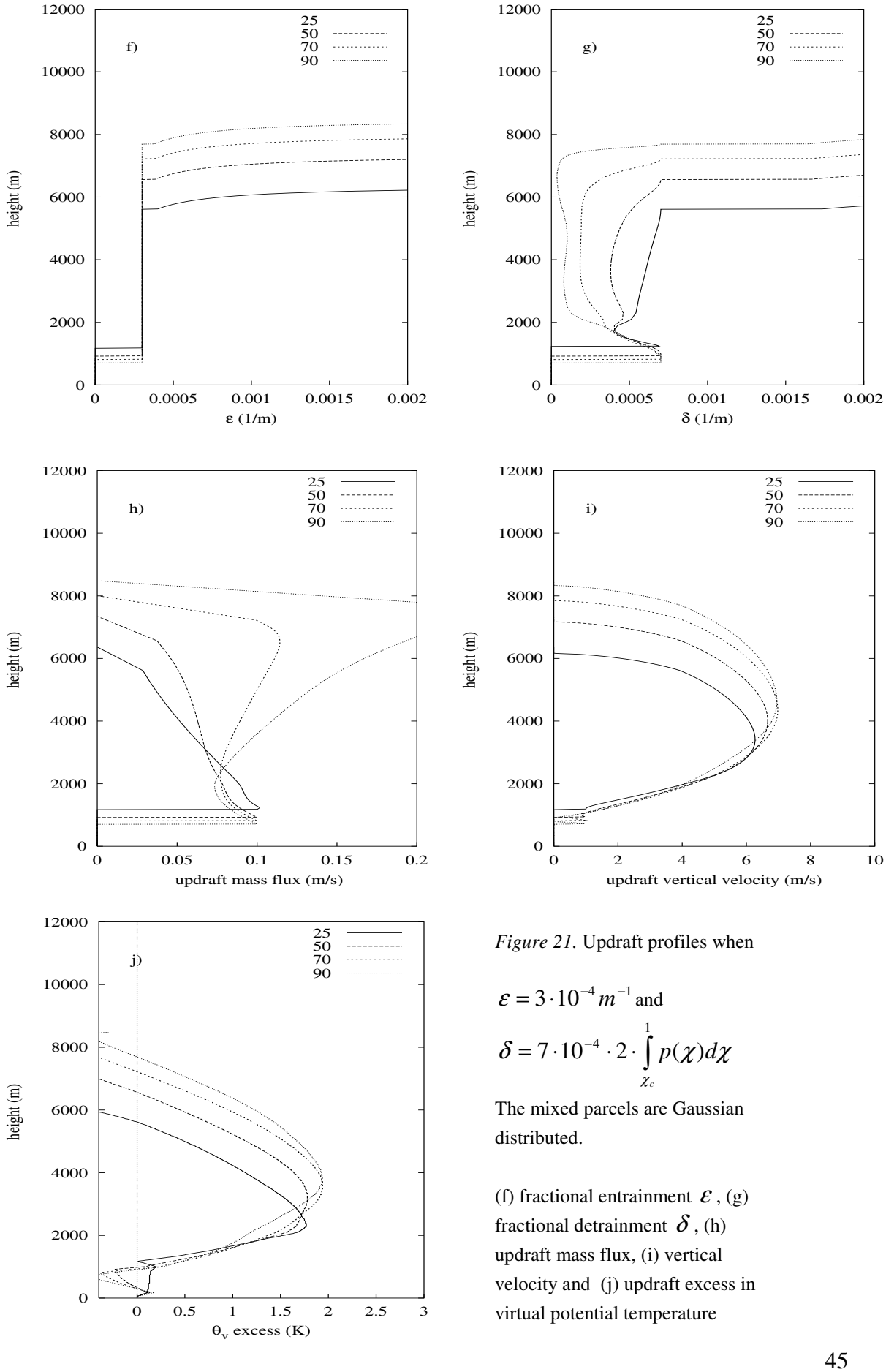

Figure 21. Updraft profiles when

$$\varepsilon = 3 \cdot 10^{-4}\, m^{-1} \text{ and}$$

$$\delta = 7 \cdot 10^{-4} \cdot 2 \cdot \int_{\chi_c}^{1} p(\chi) d\chi$$

The mixed parcels are Gaussian distributed.

(f) fractional entrainment ε, (g) fractional detrainment δ, (h) updraft mass flux, (i) vertical velocity and (j) updraft excess in virtual potential temperature

9. Discussion

9.1 On the modification to ε and δ

As can be seen in figure 21, the cloud top problem and the ϕ_c problem can be partially solved by making ε independent on the relative humidity. A simplified picture of the modified ε and δ determination is shown in figure 20. As can be seen in figure 20, the modified KF-scheme does not take the positive buoyant mixed parcels into account. As a possible explanation for this concept problem it can be assumed that the positive buoyant mixtures remain in the cloud periphery and therefore hardly contribute to the updraft mass flux. This is consistent with LES-observations that show that cloud peripheries are positively buoyant, whereas upward velocities are considerably smaller than their core values (Siebesma, 2002). Further, as can be seen in figure 19e and 19f, ε is not as sensitive to the relative humidity as δ. This is consistent with the modified KF-scheme assumption as well. However, when the positive buoyant fraction of the mixtures is neglected because it remains in the cloud periphery, it becomes hard to believe in the existence of a relative humidity – independent entrainment that *does not* ends in the cloud periphery and *does* affect the mass flux.

In a KF-update (Kain, 2002) the cloud top problem and a solution for it were already mentioned. The proposed solution states that the entraining mass is at least 50% of the environmental mass in the mixed parcels. This is - although formulated differently - the same solution to avoid the under determination of ε. No further motivation for this particular solution is given.

As can be seen in figure 21h, the magnitude of the mass flux is rather sensitive to the relative humidity. As is shown in A.8, the huge sensitivity of the updraft mass flux leads to huge sensitivity of the condensed water content (figure 21d). The mass flux sensitivity is enhanced by the adiabatic ascent assumption below the LCL. If sub-cloud entrainment is prescribed, the sensitivity of the updraft mass flux magnitude is less and therefore more realistic.

.

9.2 On the standard KF90-scheme

A parameter of the KF-scheme that requires some more attention is the environmental inflow rate. As already said, in the KF90-formulation the inflow rate is parameterized as a fraction of the updraft mass flux at the LCL. In Bretherton and McCaa, 2003, this inflow rate is set to a fraction of the local mass flux. Although no attention is paid on this considerable difference in formulation, this parameter has significant impact on the magnitude of the entrainment and detrainment profiles. Relative humidity sensitivity tests have been performed with the KF90-formulation as well and it appeared that the updraft profiles become extremely sensitive to ε_0 and the initial excesses in temperature and

moisture of the ascending parcel. These are highly unwanted features, because it is rather unclear what to prescribe for ε_0 and the initial excesses. Further, the parameterization of the inflow rate as a fraction of the local mass flux is intuitively more attractive and it is consistent with the usual parameterization of the entrainment and detrainment; see (9).

9.3 On the experiments

The standard KF-scheme fails when its moisture sensitivity is compared to the CRM-moisture sensitivity. The performance of the modified KF-scheme has to be tested more extensively, but from the sensitivity test it is clear that the modification improves the performance. A combination of the modification made in the sensitivity case and the shallow cumulus case has also been tested in the sensitivity case. In this combination ε and δ were determined according to figure 20 and the fractional inflow rate was set proportional to the inverse of height. However it is suggested by figure 19e that ε resembles a $\frac{c}{z}$- profile that is not really dependent on the relative humidity, this combination of modifications did not improve the performance.
When we consider just the shallow cumulus case, the SUM can reproduce the LES in-cloud profiles rather well. But, this is only the case when the PDF for the mixed parcels is assumed to be as asymmetric as in figure A.2 and when the fractional inflow rate is inversely proportional with height. When the standard Gaussian PDF is applied, the detrainment is highly over determined. This is noticed as well in Bretherton and McCaa, 2003. As a solution for the over determination it is proposed to involve the upward vertical velocity as well in the entrainment / detrainment determination. In this solution it is assumed that negatively buoyant mixtures can continue upward at the cost of their upward velocity. The fraction of mixed parcels that is entrained is the positive buoyant fraction and the negative buoyant fraction that continues upward and exceeds a so-called critical eddy mixing distance. This will yield a smaller detraining fraction than when only buoyancy sorting is applied. No (relative humidity) sensitivity tests with this buoyancy / momentum-sorting convection scheme have been performed. These tests are obviously more demanding on the common validity of a convection scheme than tests with one particular set of area-mean profiles. This contributes to - when the sensitivity test is concerned - the poor quantitative resemblance between the SUM-results and the CRM-results.

9.4 On the cloud model

The poor quantitative resemblance in the sensitivity test is clear when e.g. the θ_v excesses are concerned (figures 21j and 19i). Obviously, the SUM-excesses are too high. When the cloud top is concerned (figures 19g and 21h), it is clear that the SUM underdetermines the cloud top. These are problems that resemble the problems pointed out by Warner, 1970. Warner stated that (12) can not produce a realistic liquid water content and cloud top height with the same ε. When ε is increased, the excess in θ_v

decreases, but the cloud top height decreases as well. As can be seen in e.g. figure 21h, the SUM-cloud top was already low compared to the CRM-cloud tops (figure 19g).
A cloud model that does not suffer from this feature is proposed by Siebesma, 1997 and it is called the *intermittent entraining thermal*. In the cloud model that is used in the SUM, entraining air is assumed to homogenize with the cloudy air on a much shorter timescale than the typical lifetime of the cloud. Therefore, it is assumed that the entraining air in homogenized instantaneously with the cloudy air.
In the intermittent entraining thermal it is assumed that this mixing timescale is on the same order as the lifetime of the cloud. Hence, the cloud is represented as an ensemble of mixed parcels that all have different fractions of environmental air. This model will not suffer from the Warner problem, because the relatively undiluted parcels will determine the cloud top height.

10. Conclusions

It is shown that the standard KF-scheme, implemented in a single parcel ascent model is not capable to produce in-cloud fields that resemble LES-results. When the SUM is applied on one area mean profile (BOMEX) in particular, the incapability is caused by over determination of the fractional detrainment. The over determination can be solved by assuming that the mixed parcels are asymmetrically distributed instead of Gaussian, i.e. parcels with relatively much cloudy mass occur more often. The resemblance can be improved further by scaling the fractional inflow rate inversely proportional with height.

When a relative humidity sensitivity test is performed, it appears that KF decreases the fractional entrainment when the relative humidity decreases. This is not in agreement with the CRM-results and it causes the cloud excesses in ϕ and the cloud top height to react wrong on changes in the relative humidity. The wrong reaction can be improved when the fractional entrainment is assumed to be independent on χ_c. In this modified KF-scheme the fractional detrainment - that is still dependent on χ_c - determines the sensitivity of the mass flux magnitude to the relative humidity.

The improvements in sensitivity with this modification are clear, but the sensitivity resemblance with the CRM is still not very good. Further improvement could be achieved by involving upward momentum in the sorting mechanism. This will enhance the detrainment in dryer environments, because the in-cloud upward velocity is in general lower when the relative humidity is lower.

Appendix

A.1 Virtual temperature

The density ρ of an isothermal air parcel with volume V, temperature T and total mass m can be written as the sum of partial densities of respectively dry air, water vapour and liquid water.

$$\rho = \frac{m}{V} = \rho_d + \rho_v + \rho_l . \tag{a.1}$$

When we apply the gas law for dry air and water vapour we get for the partial pressures of dry air p_d and water vapour p_v

$$\begin{aligned} p_d &= \rho_d R_d T, \\ p_v &= \rho_v R_v T, \end{aligned} \tag{a.2}$$

in which R_d and R_v are the specific gas constants for dry air and water vapour.

When we add up the partial pressures and assume that the liquid water does not have an effect on the pressure we get for the total pressure p

$$p = \rho R_d T \left[1 + (\varepsilon^{-1} - 1)\frac{\rho_v}{\rho} - \frac{\rho_l}{\rho} \right]. \tag{a.3}$$

This is the equation of state for an air parcel that contains water vapour and liquid water,

where $\varepsilon = \dfrac{R_d}{R_v} \approx 0.622$.

We can rewrite (a.3) in the same form as (a.2) when we define a virtual temperature T_v

$$T_v = T\left[1 + 0.61 q_v - q_l\right]. \tag{a.4}$$

So that we obtain for the total pressure *p*

$$p = \rho R_d T_v , \tag{a.5}$$

The specific humidity for water vapour q_v and liquid water content q_l are defined as

$$q_v = \frac{\rho_v}{\rho}, \qquad q_l = \frac{\rho_l}{\rho}. \tag{a.6}$$

The virtual temperature can be interpreted as the temperature that dry air must have in order to have the same density as the moist air with the afore mentioned specific humidities. For a constant pressure, T_v is inversely proportional to the total density of a parcel, so this temperature is, given the virtual temperature of the surroundings of the parcel, a direct measurement for the buoyancy of the parcel.

From (a.4) and (a.5) it is immediately clear that at constant pressure and temperature the presence of water vapour decreases the density of a parcel and the presence of liquid water increases the density of a parcel. A typical order of magnitude for q_v is 10^{-2} kg/kg, for q_l this is 10^{-3} kg/kg, so the effect of moisture on T_v is at maximum 1 %, or 3 K, which is considerable.

A.2 Saturation mixing ratio

Water vapour condensates not necessarily if the specific humidity q_v exceeds the saturation mixing ratio q_s, but for simplicity we assume that it does. It can be written as a function of the total pressure p and the saturation vapour pressure $e_s = \rho_s R_v T$, when we apply (a.3), we get

$$q_s = \frac{\rho_s}{\rho} = \varepsilon \frac{e_s}{p + e_s(\varepsilon - 1)}, \tag{a.7}$$

where e_s is given by the integrated Clausius-Clapeyron relation that can be approximated by

$$e_s = e_0 \cdot e^{\left(a\frac{T-T_0}{T-b}\right)}, \tag{a.8}$$

with $a = 17.27$, $b = 35.96\ K$, $e_0 = 6.107 hPa$ and $T_0 = 273.15 K$. Note that this equation is only valid for temperatures above the freezing point of water T_0. When temperatures become lower than T_0, equation (a.8) is still applicable, but now with constants $a = 21.88$ and $b = 7.76\ K$.

When temperatures are below T_0, a combination of (a.7) with the old and new values is used to calculate the effective saturation-mixing ratio $q_{s,eff}$, given by

$$q_{s,eff} = \alpha q_{sw} + (1-\alpha) q_{si}. \tag{a.9}$$

Where q_{sw} and q_{si} are the saturation mixing ratios with respect to water and ice, respectively. The factor α is a function of the temperature that is equal to 1 when temperatures are above T_0 and becomes equal to zero when temperatures are equal to $253\,K$, or lower. Equation (a.9) is just a very strong simplification of reality. It is the method in witch the transition from liquid water to ice is parameterized in the ECMWF-model, the European Centre for Medium-range Weather Forecasts. The ice-mixing ratio q_i is calculated analogous to (a.9). With this method it is assumed that water is, for temperatures between T_0 and 253 K, in the so-called mixed phase. In this temperature interval the condensed water consists of liquid water and ice. In reality, the transition from liquid to solid is a highly complicated process.

A.3 Conserved quantities

The total water content of a parcel, i.e. the sum of the specific humidities for water vapour, liquid and solid water, is not dependent on phase changes. Therefore, in a mixing process it is convenient to work with this quantity, because the total water content of a mixed parcel is simply the weighted average of the total water contents of the parcels that are involved in the mixing.
For example, when two parcels $\{m_1, q_{t,1}\}$ and $\{m_2, q_{t,2}\}$ mix, the total water content of the mixed parcel $q_{t,m}$ is given by

$$q_{t,m} = \frac{m_1.q_1 + m_2.q_2}{m_1 + m_2}. \tag{a.10}$$

The liquid water temperature is a modified temperature that is - like q_t - conserved during phase change, when latent heat change effects are involved. It can be derived starting with a combination of the first and second law of thermodynamics. We can then write for the specific entropy change ds of a parcel (Siebesma, 1997)

$$ds = c_{pm} d\ln T - R_m d\ln p - \frac{L}{T} dq_l, \tag{a.11}$$

in which c_{pm}, and R_m are the parcel mean values for respectively the specific heat capacity and specific gas constant, given by $c_{pm} = c_{pd} + q_v c_{pv}$, $R_m = R_d + q_v R_v$ and L_0 is the latent heat change due to condensational effects, equal to $2.5\text{x}10^6\ J/kg$. For simplicity we use the dry air values for c_{pm} and R_m. Further, we approximate the last

term in (a.11) that represents condensational effects, by $d(L_0 \frac{q_l}{T})$. When no liquid water is involved, this term equals zero.

When we consider constant pressure, the second term on the r.h.s. of (a.11) vanishes.
For adiabatic processes the entropy of a parcel is conserved, i.e. $ds = 0$.
The liquid water temperature now follows after integration of the obtained isobaric and adiabatic form of (a.11).

$$T_l = T \cdot e^{(\frac{-L_0 q_l}{c_{pd} T})}. \tag{a.12}$$

Because liquid water mixing ratios are small, the exponent in (a.12) is small as well, so we may write as well

$$T_l \approx T - \frac{L_0}{c_{pd}} q_l. \tag{a.13}$$

When we leave liquid water out of consideration, the other terms in (a.11) define the potential temperature θ as follows: $ds = c_{pd} d \ln \theta$.

When (a.11) is integrated upward, from a reference pressure $p_0 = 1000hPa$ this gives, with $ds = 0$

$$\theta = T(\frac{p_0}{p})^{\kappa} = T\pi^{-1}, \tag{a.14}$$

with $\kappa = R_d / c_{pd} \cong 0.29$ and π the so-called Exner function.
This potential temperature θ is conserved under adiabatic pressure change, e.g. adiabatic ascent. When phase changes are included, a liquid water potential temperature θ_l can be defined by $ds = c_{pd} d \ln \theta_l$. When we again integrate the approximated form of (a.11), from $p_0 = 1000hPa$, this gives

$$\theta_l = \theta \cdot e^{(\frac{-L_0 q_l}{c_{pd} T})} = T(\frac{p_0}{p})^{\kappa} e^{(\frac{-L_0 q_l}{c_{pd} T})}. \tag{a.15}$$

This temperature is conserved under adiabatic pressure changes and phase changes, e.g. moist adiabatic ascent.

Since the exponent in (a.15) is in general much smaller than 1, θ_l can be linearized, leading to

$$\theta_l \approx \theta - \frac{L_0}{c_{pd} \pi} q_l. \tag{a.16}$$

Just like with the saturation vapour pressure, the effect of freezing has to be taken into account when temperatures are below T_0.

Freezing causes, just like condensation, the release of latent heat. Analogous to (a.9), the effective change of latent heat L_{eff} is given by

$$L_{eff} = \alpha L_0 + (1-\alpha) L_s , \tag{a.17}$$

in which L_s is the latent heat change due to sublimation, equal to $2.8\text{x}10^6 \ J/kg$.

When condensed water is involved and when precipitating clouds are concerned, precipitation has to be taken into account as well. The generation of precipitation increases when the liquid water content increases, but is also increased by other effects, such as the collection of small cloud droplets by falling rain droplets. These enhancing processes can be parameterized in terms of temperature and the precipitation rate itself.

Temperature is not influenced by precipitation, so θ_l increases when liquid or condensed water is removed by precipitation. When the amount of water that is removed is q_r, q_t decreases with q_r and θ_l must be written as

$$\theta_l \approx \theta - \frac{L_0}{c_{pd}\pi}(q_l - q_r) \tag{a.18}$$

During a mixing process, the liquid water potential temperature of the mixed parcel can be calculated analogous to (a.10). This yields the following mixing curve for θ_l and q_t .

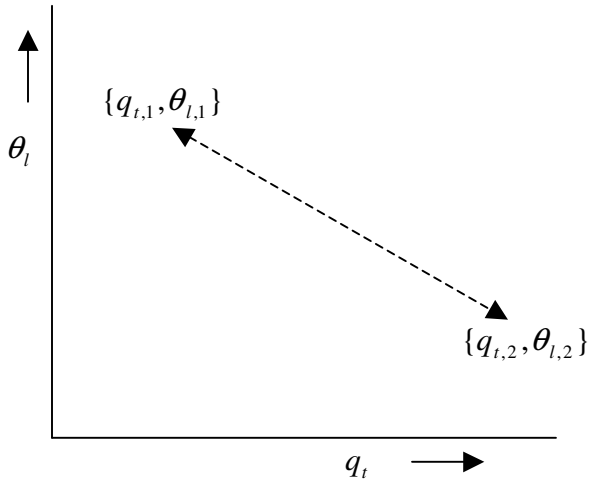

Figure A.1. For all possible mixtures of parcel 1 and 2 q_t and θ_l lay on a straight line, i.e. q_t and θ_l can be linearly mixed. This is of course only the case when there are no external sources and sinks (precipitation) of moisture and heat during the mixing.

The virtual potential temperature θ_v is - as already said in chapter 2 - obtained after combination of (a.14) and (a.4)

$$\theta_v = \theta\left[1 + 0.61 q_v - q_l\right] \tag{a.19}$$

The buoyancy force B, acting on a parcel can be defined as follows

$$B = g\,\frac{\theta_v - \overline{\theta_v}}{\overline{\theta_v}}. \tag{a.20}$$

A.4.1 The continuity equations for cloudy air

For convenience we write ϕ for both θ_l and q_t. When we assume the velocity field in a horizontal area A to be non-divergent, we can write down the continuity equation for ϕ as follows (Siebesma, 1997)

$$\frac{\partial \phi}{\partial t} + \vec{\nabla}_h \cdot \vec{v}\phi + \frac{\partial w\phi}{\partial z} = \vec{S}. \tag{a.21}$$

In which $\vec{v}$ is the horizontal component and w the vertical component of the velocity vector. All sources and sinks of ϕ are represented by $\vec{S}$. The density of the air is set to 1 kg/m^3 and is absorbed is $\vec{S}$. When we average the cloudy part of the first and last term on the LHS of (a.20) over area A by integrating over cloudy area $A_c(z,t)$ and applying the theorem of Leibnitz, we can write

$$\begin{aligned}
\frac{1}{A}\int_{A_c} \frac{\partial \phi}{\partial t}\,dxdy &= \frac{\partial a_c \phi_c}{\partial t} - \phi_{\partial c}\,\frac{\partial a_c}{\partial t}, \\
\frac{1}{A}\int_{A_c} \frac{\partial w\phi}{\partial z}dxdy &= \frac{\partial a_c\,\overline{w\phi}^{c}}{\partial z} - \overline{w\phi}^{\partial c}\,\frac{\partial a_c}{\partial z}.
\end{aligned} \tag{a.22}$$

The cloudy region average for ϕ is given by $\phi_c = \frac{1}{A_c}\int_{A_c} \phi dxdy$ and the fractional cloud area a_c is given by $a_c = \frac{A_c}{A}$.

The subscripts ∂c and c denote respectively the horizontal boundary and the horizontal area of the cloud and the overbars denote the spatial averages over this boundary or area.

When we substitute (a.22) in (a.21) and also take the spatial average of the cloudy part of the second term on the l.h.s. of (a.20) we find

$$\frac{\partial a_c \phi_c}{\partial t} - \phi_{\partial c} \frac{\partial a_c}{\partial t} + a_c \overline{\vec{\nabla}_h \cdot \vec{v}\phi}^{c} + \frac{\partial a_c \overline{w\phi}^{c}}{\partial z} - \overline{w\phi}^{\partial c} \frac{\partial a_c}{\partial z} = a_c S_c. \tag{a.23}$$

When ϕ is set to 1 and S_c to 0, (a.23) yields the continuity equation for a_c.

$$\frac{\partial a_c}{\partial t} - \frac{\partial a_c}{\partial t} + a_c \overline{\vec{\nabla}_h \cdot \vec{v}}^{c} + \frac{\partial a_c w_c}{\partial z} - w_{\partial c} \frac{\partial a_c}{\partial z} = 0 \tag{a.24}$$

When we apply the divergence theorem, (a.24) can be written in a more comprehensive form.

$$\frac{\partial a_c}{\partial t} + \frac{1}{A} \oint_{\partial c} \hat{n} \cdot (\vec{u} - \vec{u}_{\partial c}) dl + \frac{\partial a_c w_c}{\partial z} = 0. \tag{a.25}$$

In which $\hat{n}$ is the outward pointed unit normal vector at the cloud edge, $\vec{u}$ is the full velocity vector and $\vec{u}_{\partial c}$ is the velocity vector of the cloud edge itself.

We can do the same with equation (a.23), to obtain a more comprehensive form for the spatial averaged continuity equation of ϕ_c.

$$\frac{\partial a_c \phi_c}{\partial t} + \frac{1}{A} \oint_{\partial c} \hat{n} \cdot (\vec{u} - \vec{u}_{\partial c}) \phi dl + \frac{\partial a_c \overline{w\phi}^{c}}{\partial z} = a_c S_c \tag{a.26}$$

When we want to implement the definitions of detrainment and entrainment into (a.25) and (a.26), first some interpretation of these equations is needed.

The first term in (a.25) denotes the change in time of cloudy mass. The second term denotes the mass exchange across the cloudy edge and the third term the vertical advection of cloudy mass. As already mentioned, entrainment is the flux of environmental mass into the cloud and detrainment is the flux of cloudy mass into the environment. Thus, the net flux of mass out of the cloud is the difference between the detrainment and entrainment. So we can write (a.25) as

$$\frac{\partial a_c}{\partial t} + (D - E) + \frac{\partial a_c w_c}{\partial z} = 0. \tag{a.27}$$

In which D represents the detrainment and E the entrainment. Note that D - E equals zero if the cloud is advected by the wind, i.e. if $\vec{u} - \vec{u}_{\partial c}$ equals zero.

When we want to employ D and E in (a.26), we have to make an approximation first. This approximation yields that E transports average environmental properties ϕ_e into the cloud and, vice versa, D transports average cloud properties ϕ_c, out of the cloud, into the environment, independent of ϕ itself. In other words: $E_\phi = E$ and $D_\phi = D$. With this assumption, (a.26) can be written as

$$\frac{\partial a_c \phi_c}{\partial t} - E\phi_e + D\phi_c + \frac{\partial a_c \overline{w\phi}^c}{\partial z} = a_c S_c. \tag{a.28}$$

The environmental, complementary part of (a.28) can be written as

$$\frac{\partial (1-a_c)\phi_e}{\partial t} + E\phi_e - D\phi_c + \frac{\partial (1-a_c)\overline{w\phi}^e}{\partial z} = (1-a_c)S_e. \tag{a.29}$$

The assumption that leads to (a.28) and (a.29) has been tested with LES results, using a typical shallow cumulus regime dataset. (Siebesma, 1997) These results show that E and D are indeed rather independent on ϕ.

A.4.2 Updraft mass flux and dilution equations

When we want to find a practical parameterization for the updraft properties, three further approximations to (a.28) and (a.29) have to be made:

- The mass flux approximation: $\overline{w\phi}^c \cong w_c \phi_c$,
- The core cover a_c is much smaller than 1, so that $\phi_e \cong \bar{\phi}$,
- The cloud ensemble is in steady state, so $\frac{\partial a_c \phi_c}{\partial t} = 0$.

With these assumptions (a.28) and (a.29) can be written as

$$\frac{\partial M}{\partial z} = E - D, \tag{a.30}$$

$$\frac{\partial M \phi_c}{\partial z} = E\bar{\phi} - D\phi_c. \tag{a.31}$$

The mass flux M is usually given by $M = \rho_c a_c w_c$, but because E and D are fractions of M the dependency of M on ρ, a and w cancels out, according to (a.30). This makes the profile of M independent on the profiles of ρ, a and w.

The approximation $a_c << 1$ can be made to (a.29) as well, in order to obtain

$$\frac{\partial \overline{\phi}}{\partial t} = -E\overline{\phi} + D\phi_c - \frac{\partial (1-a_c) w_e \phi_e}{\partial z} + \overline{S}. \tag{a.32}$$

It can be understood out of principles of continuity that the average and in-cloud vertical velocities must be linked according to

$$(1-a_c) w_e + a_c w_c \cong 0. \tag{a.33}$$

In other words: what goes up must come down. When (a.31), the definition of mass flux and (a.33) are applied to (a.32), the tendency for the average profile is given by

$$\frac{\partial \overline{\phi}}{\partial t} = -\frac{\partial M (\phi_c - \overline{\phi})}{\partial z} + \overline{S} \tag{a.34}$$

Note that according to the second term on the r.h.s. of (a.34) the turbulent flux $\overline{w\phi}^c$ is approximated by $M(\phi_c - \overline{\phi})$, which makes intuitively sense. This approximation provides - although it is a strong simplification - a good representation of this term, as can be deduced from LES results (Siebesma and Cuijpers, 1995).

A.6 Determination of χ_c

The calculation of χ_c can – of course - be done numerically. The liquid water, water vapour content and temperature of the mixtures can be derived from their total water content and liquid water temperature by linear expansion. More details on the applied condensation scheme are given in Cuijpers, 1994.

The analytic method to determine χ_c is summarized below. It applies well when temperatures above T_0 are considered. In the mixed phase, the latent heat exchange becomes a function of the mixed parcel temperature; when this effect is not taken into account, this yields an error in χ_c of 10 % at max, which is considerable. When this effect is taken into account, this will make the expression for $\theta_v(\chi)$ implicit and hence less interesting for application.

The derivation of the equation that describes the updraft virtual potential temperature as a function of χ is rather laborious, so only the most important steps are given.

As mentioned before, θ_l and q_t can be linearly mixed. Hence, we can write $\theta_l(\chi)$ and $q_t(\chi)$ as follows

$$\theta_l(\chi) = \theta_{l,u} + \chi(\theta_{l,e} - \theta_{l,u}) \tag{a.35}$$

$$q_t(\chi) = q_{t,u} + \chi(q_{t,e} - q_{t,u}) \tag{a.36}$$

The subscripts *u* and *e* denote the updraft and environment, respectively.

We can write, according to (a.19) and (a.15) the virtual potential temperature of the mixture $\theta_v(\chi)$ as

$$\theta_v(\chi) = \theta_l(\chi)\left[1 + \varepsilon q_t(\chi) - (1+\varepsilon) q_l(\chi)\right] + \frac{\alpha}{\pi} q_l(\chi). \tag{a.37}$$

Terms that are not linear in q_t or q_l are neglected and $\frac{L}{c_p}$ is denoted with α.

The next aim is to find an expression for $q_l(\chi)$. In general, we may write

$$q_l(\chi) = q_t(\chi) - q_s(T(\chi)) \tag{a.38}$$

We can find $q_s(T(\chi))$ by linear expansion from $q_s(T_u)$. After substitution, some rewriting and collection of terms up to order χ we find in the end.

$$\theta_v(\chi) = \theta_{v,u} + \chi\left[\frac{\varepsilon\gamma - 1}{1+\gamma}\theta_{l,u} + \frac{1}{(1+\gamma)}\frac{\alpha}{\pi}\right](q_{t,e} - q_{t,u}) + \chi\left[\frac{1}{1+\gamma} + \frac{T_{l,u}(1+\varepsilon)\gamma}{(1+\gamma)}\frac{1}{\alpha}\right](\theta_{l,e} - \theta_{l,u})$$

(a.39)

In which the factor $\frac{L}{c_p}\frac{\partial q_s}{\partial T}\Big|_{T_u}$ is denoted as γ.

The remarkable property of mixed dry and moist air is that for different relative humidities - and when all other variables are kept equal - the distinct virtual potential temperature differences of the mixed parcels and their environment all intersect at the same mixing fraction, as can be seen in figure 15. The concerning value of χ is called χ_{cross}. It is given by

$$\chi_{cross} = \frac{\varepsilon\theta_e}{B} \tag{a.40}$$

in which B is the first term between brackets on the r.h.s. of (a.39) i.e.

$$B = \frac{\varepsilon\gamma - 1}{1+\gamma}\theta_{l,u} + \frac{1}{(1+\gamma)}\frac{\alpha}{\pi} \tag{a.41}$$

De Roode, 2004, gives more details on the analytic analysis of mixing of moist air.

A.7 Entrainment and detrainment prescription.

The entrainment and detrainment are dependent on the inflow rate $\varepsilon_0 M_u$, χ_c and the PDF for the mixed parcels. In order to do the derivation analytically, only the straight PDF and asymmetric PDF are considered. These PDFs as well as the Gaussian PDF are depicted in figure A.2

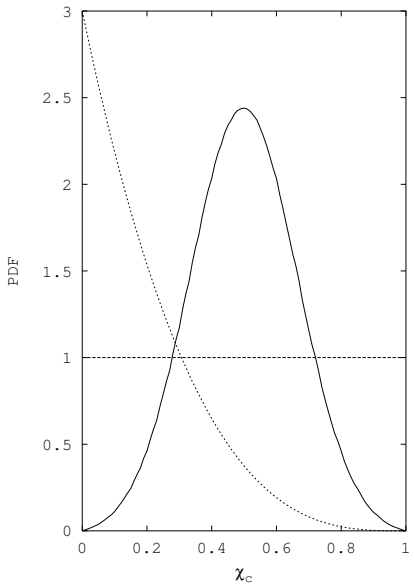

Figure A.2. plots of the Gaussian (solid), straight (dashed) and asymmetric (dotted) PDFs. The Gaussian PDF is truncated at 0 an 1 and has a standard deviation that is set to 1/6.

During the mixing process a fraction of environmental air and a fraction of updraft air mix in the so-called transition region to form mixed parcels with total mass dM_t (figure A.3).

When we consider the straight PDF, i.e. $p(\chi) = 1$, the fraction of environmental air in the mixed parcels is given by

$$dM_e = \varepsilon_0 M_u dz = \int_0^1 dM_t \chi p(\chi) d\chi \tag{a.42}$$

or

$$dM_t = 2\varepsilon_0 M_u dz = 2dM_e \tag{a.43}$$

So, as expected, the fraction of updraft air in the mixture $dM_t - dM_e$ is equal to the fraction environmental air in the mixed parcels.

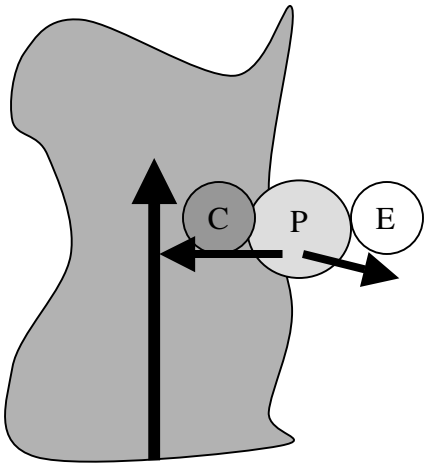

Figure A.3. Different parcels; Cloudy C and Environmental E with total mass $\varepsilon_0 M_u dz$ mix in the cloud periphery to form distinct mixed parcels P, with total mass dM_t. The cloudy and environmental parcels are only equal in mass, when the PDF for the mixed parcels is symmetric around 0.5.

For $dz = 1$, each parcel with mixing fraction χ that is entrained has a mass contribution to the updraft as follows

$$dE = 2\varepsilon_0 M_u \chi p(\chi) d\chi \tag{a.44}$$

All mixtures that have a mixing fraction less then χ_c are entrained, so the entrainment can be written as

$$E = 2\varepsilon_0 M_u \int_0^{\chi_c} \chi p(\chi) d\chi = \varepsilon_0 M_u \chi_c^2. \tag{a.45}$$

Analogous, each parcel with χ greater then χ_c yields the following detrainment contribution

$$dD = 2\varepsilon_0 M_u (1-\chi) p(\chi) d\chi, \tag{a.46}$$

which gives for the detrainment after mixing

$$D = 2\varepsilon_0 M_u \int_{\chi_c}^{1} (1-\chi) p(\chi) d\chi = \varepsilon_0 M_u (1-\chi_c)^2. \tag{a.47}$$

When then usual parameterizations for E and D (9) are substituted in (a.45) and (a.47), we find for ε and δ

$$\begin{aligned} \varepsilon &= \varepsilon_0 \chi_c^2 \\ \delta &= \varepsilon_0 (1-\chi_c)^2. \end{aligned} \tag{a.48}$$

We can do the same procedure for the asymmetric PDF given by $p(\chi) = 3(1-\chi)^2$ to find

$$dM_e = \varepsilon_0 M_u dz = \int_0^1 dM_t \chi p(\chi) d\chi, \tag{a.49}$$

or

$$dM_t = 4\varepsilon_0 M_u dz = 4dM_e. \tag{a.50}$$

The fractional entrainment can be found by applying the same procedure as with the straight PDF. This yields, after some writing

$$\begin{aligned} \varepsilon &= \varepsilon_0 (\chi_c^4 - 2\tfrac{2}{3}\chi_c^3 + 2\chi_c^2) \\ \delta &= \varepsilon_0 (1-\chi_c)^4. \end{aligned} \tag{a.51}$$

In chapter 5 it is noticed that ε and δ do not add up to dM_t. One might wonder what happens to the remaining mass. When we zoom in to figure A.3, the disappeared mass can be traced, see figure A.4.

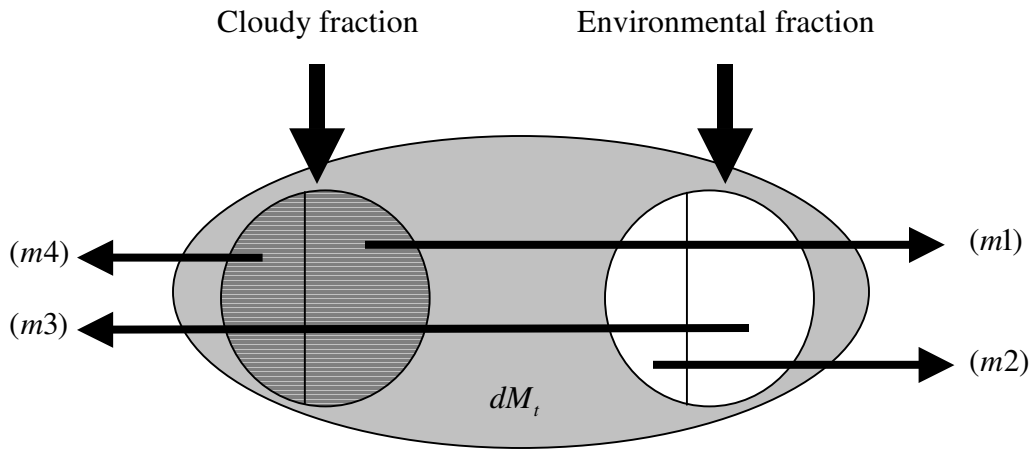

Figure A.4. Magnification of the ensemble mixed parcels P in figure A.3. The cloudy and environmental fractions consist of two fractions themselves.

For the determination of ε and δ we are only interested in masses ($m3$) and ($m1$) The masses ($m4$) and ($m2$) do not contribute to the entrainment and detrainment. This is because ($m4$) is already cloudy air and ($m2$) is already environmental air. For convenience, the magnitudes of the masses are given for a straight PDF. Though, the principle holds for any PDF.

$$
\begin{aligned}
m1 = D &= dM_t \int_{\chi_c}^{1} (1-\chi)d\chi = \tfrac{1}{2} dM_t (1-\chi_c)^2 \\
m2 &= dM_t \int_{\chi_c}^{1} \chi d\chi = \tfrac{1}{2} dM_t (1-\chi_c^2) \\
m3 = E &= dM_t \int_{0}^{\chi_c} \chi d\chi = \tfrac{1}{2} dM_t \chi_c^2 \\
m4 &= dM_t \int_{0}^{\chi_c} (1-\chi)d\chi = -\tfrac{1}{2} dM_t (1-\chi_c)^2 + \tfrac{1}{2} dM_t
\end{aligned}
\qquad \text{(a.52a)}
$$

When the four distinct masses are added up, this yields dM_t, so the mass is continuous during the mixing, as it should be.

When the modification to the determination of ε and δ as proposed in figure 20 is considered, we can repeat the before mentioned procedure to show that the mass of the mixed parcels is continues during the mixing. Figure A.4 now becomes

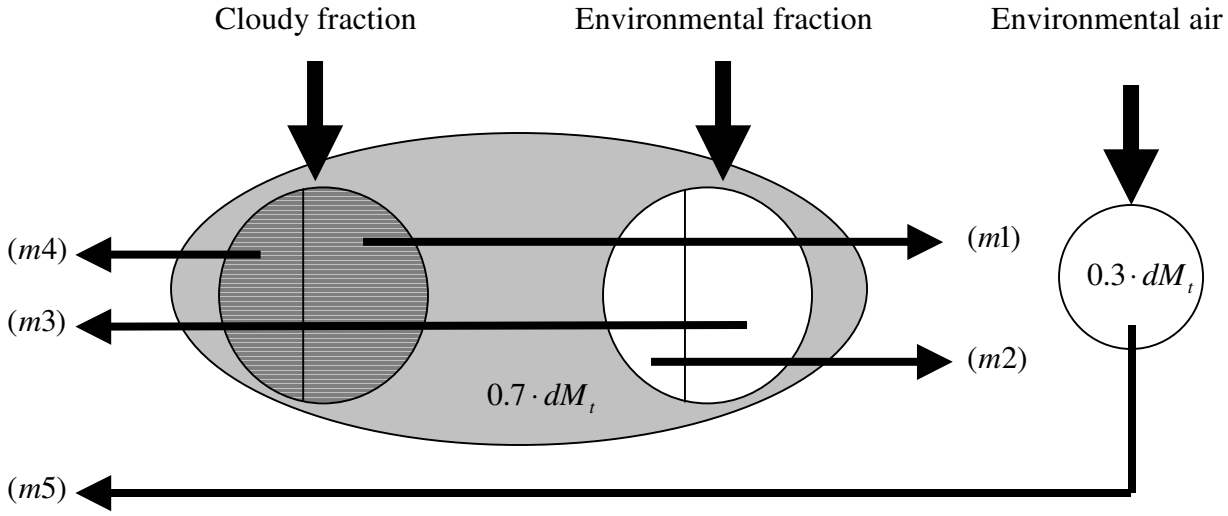

Figure A.5. The modified determination of *E* and *D*. A portion air with mass $0.3 \cdot dM_t$ entrains, no matter what the properties of the mixed parcels are.

It is assumed that the portion air that entrains no matter what and the portion air that forms mixed parcels relate according to $0.3dM_t$ and $0.7dM_t$, respectively. This yields a total air portion of dM_t. The sum of *E* and *D* should give dM_t as well. We find, according to figure A.5.

$$
\begin{aligned}
m1 = D &= 0.7 \cdot dM_t \int_{\chi_c}^{1} (1-\chi) d\chi = \tfrac{1}{2} \cdot 0.7 \cdot dM_t (1-\chi_c)^2 \\
m2 &= 0.7 \cdot dM_t \int_{\chi_c}^{1} \chi d\chi = \tfrac{1}{2} \cdot 0.7 \cdot dM_t (1-\chi_c^2) \\
m3 = E &= 0.7 \cdot dM_t \int_{0}^{\chi_c} \chi d\chi = \tfrac{1}{2} \cdot 0.7 \cdot dM_t \chi_c^2 \\
m4 &= 0.7 \cdot dM_t \int_{0}^{\chi_c} (1-\chi) d\chi = -\tfrac{1}{2} \cdot 0.7 \cdot dM_t (1-\chi_c)^2 + \tfrac{1}{2} \cdot 0.7 \cdot dM_t \\
m5 = E &= 0.3 \cdot dM_t
\end{aligned}
\qquad \text{(a.52b)}
$$

Masses *m*2, *m*3 and *m*4 are neglected in the modification. This is of no consequence when *m*2 and *m*4 are considered, because these masses did not contribute to *E* and *D* anyway. A weakness of the modification is the neglect of *m*3. This mass is replaced by *m*5. At the moment, the only argument that can be given to justify this neglect is given by figure 19e. This figure states that ε is not substantially dependent on the relative humidity. This motivates the use of a fractional entrainment that is independent of χ_c. The question that is yet to be answered is what happens to *m*3.

A.8 Precipitation, vertical velocity and cloud top

To determine the amount of water that is removed by precipitation, we use a parameterization of Sundqvist, 1978, that assumes that the generation of precipitation G_{mw} in pure water and mixed phase clouds can be written as

$$G_{mw} = ac_0 q_c \left[1 - e^{-(\frac{q_c}{q_{crit}})^2} \right] \tag{a.53}$$

In which a is the fractional cloud cover, c_0^{-1}, typically 10^{-4} s^{-1} is a conversion time scale and q_{crit}, typically 0.3 g kg^{-1} is a critical condensed water content from which the generation begins to be significant. This is of course a strong simplification of reality. The condensed water content q_c is the sum of q_i and q_l. The generation has unit s^{-1}. When it is implemented in (a.30) and rewritten in the same form as the dilution equation (12), we obtain for q_t

$$\frac{\partial q_{t,c}}{\partial z} = \varepsilon(\overline{q_t} - q_{tc}) - \frac{G_{mw}}{M} \tag{a.54}$$

This means that the effect of precipitation on the profile of q_t is depended on the magnitude of the local mass flux. This is because the generation of precipitation is not depended on the magnitude of the upward flux of q_t. Therefore, the precipitation has more impact on the profile of q_t when the upward mass flux is smaller. This is because the size of the sink (precipitation) is relatively greater compared to the source (upward flux) of q_t.

Vertical velocity and cloud top

In the SUM the cloud top height is defined as the height at which the upward velocity becomes zero. The upward velocity w is determined with

$$\frac{1}{2}\frac{\partial w_c^{\,2}}{\partial z} = -b\varepsilon w_c^2 + aB \tag{a.55}$$

Turbulence storage and the effects of pressure perturbation are absorbed in the so-called fetch-factors a and b. In the SUM these factors are set to 1 and 2, respectively.
As can be seen in equations (11) and (20), the cloud overshoot scales with ε_0^{-1}.
This leads, obviously to too much mass flux overshoot, since ε_0 has a typical value of 10^{-3} - 10^{-4} m^{-1}. Therefore, above the LZB, ε_0 is set to

$$\varepsilon_0 = \frac{-1}{z_t - z}. \qquad \text{(a.56)}$$

In which z_t is the cloud top height. This yields a linearly decreasing mass flux that becomes zero at the cloud top.

References

Bretherton, C.S, McCaa, J.R. and Grenier, H.,2003: *A new parameterization for shallow cumulus convection and its application to marine subtropical cloud-topped boundary layers*

Monthly weather review, Dec 2001

Cuijpers, J.W.M.,1994: *Large-Eddy simulation of cumulus convection*

PhD thesis

Frank, W.M. and Cohen, C., 1985: *Properties of tropical cloud ensembles estimated using a cloud model and an observed updraft population.*

Journal of the atmospheric sciences vol. 42

Johnson, R.H., 1977: *The effects of cloud detrainment on the diagnosed properties of cumulus populations*

Journal of the atmospheric sciences vol. 34

Kain, J.S. and Fritsch, M, 1990: *A one-dimensional entraining/detraining plume model and its application in convective parameterization*

Journal of the atmospheric sciences vol. 47

Lord, S.J., 1982: *Interactions of a cumulus cloud ensemble with the large-scale environment*

Journal of the atmospheric sciences vol. 39

Neggers, R., 2002: *Shallow cumulus convection*

PhD thesis 2002

Paluch, I.R., and Knight, C.A., 1989: *Entrainment and fine scale mixing in continental convective cloud.*

Journal of the atmospheric sciences vol. 46

Rogers, D.P.J.W., Telford and Chai, S.K.,1985: *Entrainment and development of the microphysics of convective clouds.*

Journal of the atmospheric sciences vol. 42

De Roode, S., 2004: *Buoyancy reversal in cumulus clouds*

Journal of the atmospheric sciences August 2004.

Siebesma, A.P., 1997: *Shallow cumulus convection*

Buoyant convection in geophysical flows 441

Siebesma, A.P., 2003: *A large eddy simulation intercomparison study of shallow cumulus convection*
Journal of the atmospheric sciences vol. 60

Siebesma, A.P. and Holtslag A.A.M., 1996: *Model impacts of entrainment and detrainment rates in shallow cumulus convection*
Journal of the atmospheric sciences vol. 53

Simpson, J., 1983: *Cumulus clouds: interactions between laboratory experiments and observations as foundations for models*
Mesoscale meteorology 392

Warner, J., 1970: *On steady-state one-dimensional models of cumulus convection*
Journal of the atmospheric sciences vol. 27